PLOS PATHOGENS

RESEARCH ARTICLE

A unique GCN5 histone acetyltransferase complex controls erythrocyte invasion and virulence in the malaria parasite *Plasmodium falciparum*

Jun Miao[1]*, **Chengqi Wang**[2], **Amuza Byaruhanga Lucky**[1], **Xiaoying Liang**[1], **Hui Min**[1], **Swamy Rakesh Adapa**[2], **Rays Jiang**[2], **Kami Kim**[1], **Liwang Cui**[1]*

1 Department of Internal Medicine, Morsani College of Medicine, University of South Florida, Tampa, Florida, United States of America, **2** Center for Global Health and Infectious Diseases Research, College of Public Health, University of South Florida, Tampa, Florida, United States of America

* jmiao1@usf.edu (JM); liwangcui@usf.edu (LC)

Abstract

The histone acetyltransferase GCN5-associated SAGA complex is evolutionarily conserved from yeast to human and functions as a general transcription co-activator in global gene regulation. In this study, we identified a divergent GCN5 complex in *Plasmodium falciparum*, which contains two plant homeodomain (PHD) proteins (PfPHD1 and PfPHD2) and a plant apetela2 (AP2)-domain transcription factor (PfAP2-LT). To dissect the functions of the PfGCN5 complex, we generated parasite lines with either the bromodomain in PfGCN5 or the PHD domain in PfPHD1 deleted. The two deletion mutants closely phenocopied each other, exhibiting significantly reduced merozoite invasion of erythrocytes and elevated sexual conversion. These domain deletions caused dramatic decreases not only in histone H3K9 acetylation but also in H3K4 trimethylation, indicating synergistic crosstalk between the two euchromatin marks. Domain deletion in either PfGCN5 or PfPHD1 profoundly disturbed the global transcription pattern, causing altered expression of more than 60% of the genes. At the schizont stage, these domain deletions were linked to specific down-regulation of merozoite genes involved in erythrocyte invasion, many of which contain the AP2-LT binding motif and are also regulated by AP2-I and BDP1, suggesting targeted recruitment of the PfGCN5 complex to the invasion genes by these specific factors. Conversely, at the ring stage, PfGCN5 or PfPHD1 domain deletions disrupted the mutually exclusive expression pattern of the entire *var* gene family, which encodes the virulent factor PfEMP1. Correlation analysis between the chromatin state and alteration of gene expression demonstrated that up- and down-regulated genes in these mutants are highly correlated with the silent and active chromatin states in the wild-type parasite, respectively. Collectively, the PfGCN5 complex represents a novel HAT complex with a unique subunit composition including an AP2 transcription factor, which signifies a new paradigm for targeting the co-activator complex to regulate general and parasite-specific cellular processes in this low-branching parasitic protist.

Author summary

Epigenetic regulation of gene expression plays essential roles in orchestrating the general and parasite-specific cellular pathways in the malaria parasite *Plasmodium falciparum*. To better understand the epigenetic mechanisms in this parasite, we characterized the histone acetyltransferase GCN5-mediated transcription regulation during intraerythrocytic development of the parasite. Using tandem affinity purification and proteomic characterization, we identified that the PfGCN5-associated complex contains nine core components, including two PHD domain proteins (PfPHD1 and PfPHD2) and an AP2-domain transcription factor, which is divergent from the canonical GCN5 complexes evolutionarily conserved from yeast to human. To understand the functions of the PfGCN5 complex, we performed domain deletions in two subunits of this complex, PfGCN5 and PfPHD1. We found that the two deletion mutants displayed very similar growth phenotypes, including significantly reduced merozoite invasion rates and elevated sexual conversion. These two mutants were associated with dramatic decreases in histone H3K9 acetylation and H3K4 trimethylation, which led to global changes in chromatin states and gene expression. Consistent with the phenotypes, genes significantly affected by the PfGCN5 and PfPHD1 gene disruption include those participating in parasite-specific pathways such as invasion, virulence, and sexual development. In conclusion, this study presents a new model of the PfGCN5 complex for targeting the co-activator complex to regulate general and parasite-specific cellular processes in this low-branching parasitic protist.

Introduction

Packaging of the eukaryotic genomes with nucleosomes into chromatin affects all essential cellular processes such as transcription, DNA replication, and repair. A key mechanism for regulating chromatin structure involves post-translational modifications (PTMs) of nucleosomal histones, which can alter the accessibility of DNA and recruit distinct PTM readers and other effector proteins [1]. A multitude of histone PTMs such as acetylation, methylation, phosphorylation, ubiquitination, and sumoylation act sequentially or combinatorially to create a "histone code" to facilitate or repress chromatin-mediated transcription [2–6]. Histone acetylation, a major PTM, is catalyzed by the histone acetyltransferase (HAT) enzymes and is correlated with active transcription [7]. HAT enzymes exist in large multimeric protein complexes such as the best-studied SAGA (Spt-Ada-Gcn5 acetyltransferase) complex [8], which is evolutionarily conserved from yeast to humans. The SAGA complex is composed of 18–20 subunits, which are organized into functional modules including the HAT catalytic core, a histone de-ubiquitinase module, the TATA-binding protein (TBP) regulatory module, and the structural module [9]. In other SAGA-like complexes such as the ATAC (ADA two A-containing) complex, the HAT catalytic core, consisting of the GCN5 acetyltransferase, ADA2, ADA3, and Sgf29, is conserved [9,10]. Surprisingly, the GCN5 complexes in the apicomplexan parasites, a group of early-branching eukaryotes including the malaria parasites and *Toxoplasma gondii*, appear to have diverged significantly from the SAGA complexes. In *Toxoplasma gondii*, TgGCN5b was found to interact with ADA2 and the plant apetela2 (AP2)-domain-containing transcription factors (TFs), while the parasite lacks most of the conserved SAGA components [11,12]. Interestingly, although the SAGA complex in plants is highly conserved, plants also use certain AP2-domain TFs to recruit the SAGA complex to cold stress genes [13,14]. Earlier studies suggested that SAGA regulates about 10% of genes in yeast and plants [15,16], but a

recent revisit of this issue in yeast revealed ubiquitous localization of SAGA at all gene promoters and reduced transcription of nearly all genes upon the disruption of SAGA [17,18]. From these studies, SAGA appears to act as a general co-activator for all RNA polymerase II transcription, and its methyl reader (Sgf29) and acetyl reader (GCN5) subunits build synergistic crosstalk to coordinate transcription. As a co-activator complex that functions in the recruitment of the preinitiation complex, SAGA plays essential roles in metazoan development [19].

The human malaria parasite *Plasmodium falciparum*, caused nearly half a million deaths in 2019 alone [20]. Its intricate lifecycle involving a vertebrate host and a mosquito vector requires precise regulation of transcription to cope with the comprehensive developmental program and environmental changes during host transitions [21–23]. Accumulating evidence indicates that the malaria parasite harbors unusual properties of transcriptional regulation that are divergent from other eukaryotes even for the conserved TFs [24–28]. For example, although the *Plasmodium* genome encodes the major components of the general transcription machinery, there is a general deficiency of specific *Plasmodium* TFs [29,30]. Compared to the similarly-sized genome of yeast *Saccharomyces cerevisiae* with ~170 specific TFs [31], the *P. falciparum* genome only has ~30 TFs, including the 27 AP2-domain TFs [30,32,33]. In contrast, *P. falciparum* has almost the full complement of chromatin proteins, consistent with the notion that epigenetic regulation is a key component of malaria biology [27,34]. One distinct feature of the *P. falciparum* epigenome is that it consists mainly of euchromatin, with restricted heterochromatin regions at subtelomeres and a few internal loci [35–41]. The heterochromatin clusters localize to the nuclear periphery and are demarcated by high levels of H3K9me3 and binding of heterochromatin protein 1 (HP1). These heterochromatin regions control antigenic variation, drug sensitivity, and gametocyte production [35,36,41–46]. In comparison, the *Plasmodium* euchromatin is characterized by low or no nucleosome occupancy at the transcription start sites (TSSs) and core promoters of highly expressed genes, which exhibit cyclic changes during the intraerythrocytic development cycle (IDC) [47–52]. Euchromatin is marked with the active histone PTMs such as H3K9ac, H4K8ac, and H3K4me3 [36,53,54], presumably deposited by the HAT enzymes PfGCN5 and PfMYST, and the methyltransferase PfSET1, respectively [55–58]. Of these euchromatic marks, H3K9ac at the promoter regions correlates well with the transcriptional status of the genes, whereas H3K4me3 shows stage-specific regulation and does not correlate with transcription [54]. Despite the importance of the euchromatin structure, as evidenced by the essence of the "writers" of these histone marks [57,59], the mechanisms by which these active histone marks are deposited, maintained, and dynamically regulated during development are unknown. More intriguingly, since most of the genes encoding the diverse cellular pathways reside in the euchromatic regions, it is not clear how the cascade-like gene expression pattern observed during the IDC is achieved.

The *P. falciparum* genome encodes a single GCN5 protein, PfGCN5, with a long, unique N-terminal extension lacking similarity to known protein domains, and a conserved C-terminal HAT enzyme domain that can acetylate histone H3 at K9 and K14 *in vitro* [55]. During the IDC, PfGCN5 is present as a full-length form, which also undergoes proteolytic processing by a cysteine protease-like enzyme [60]. PfGCN5 is essential for the IDC of the parasites; thus, its function has been probed by chemical inhibition of its activity, which caused overall disturbance of transcription and gross reduction of H3K9ac, establishing a potential link between PfGCN5 and H3K9ac in the parasite [56,61]. Recent efforts aiming to identify "readers" of the PTMs in *P. falciparum* led to the identification of putative PfGCN5-associated protein complex(es), which is highly divergent from the evolutionarily conserved SAGA complex [62]. Here, we used a tandem affinity purification (TAP) procedure to define a unique PfGCN5 complex and then we performed functional analyses of its key subunits. This work established the essential functions of this PfGCN5 complex in regulating cellular and metabolic pathways

critical for parasite-specific processes such as antigenic variation, erythrocyte invasion, and sexual development.

Results

PfGCN5 forms a unique complex that is highly divergent from the SAGA complex

The evolutionarily conserved SAGA complex in eukaryotes is composed of 18–20 subunits, which are organized into several modules including the HAT catalytic core consisting of GCN5, ADA2, ADA3, and Sgf29 [9,10]. By contrast, bioinformatic analysis of the *Plasmodium* genomes using conserved modular components of the SAGA complexes identified only two ubiquitous subunits, GCN5 and ADA2 [55,63], and a potential Tra1 homolog (PF3D7_1303800) [64], suggesting that the GCN5 complex(es) in these early-branching, parasitic protists might be highly divergent from the SAGA complex. Our recent work, aiming to identify "readers" of modified histones with the H3K4me3 peptide, surprisingly pulled down a putative PfGCN5 complex containing the PfGCN5, PfADA2, and two large proteins containing multiple plant homeodomains (PHDs), namely PfPHD1 and PfPHD2 [62]. To precisely define the GCN5 complex(es) in *P. falciparum*, we tagged the C-terminus of the endogenous *PfGCN5* gene in the 3D7 strain with a PTP tag consisting of a protein C epitope, a tobacco etch virus (TEV) protease cleavage site, and two protein A domains (**S1A and S1B Fig**), which allows for efficient TAP of protein complexes under native conditions with extremely low backgrounds [65,66]. Integration-specific PCR confirmed the correct integration of the *PTP* tag at the *PfGCN5* locus (**S1C Fig**). The transgenic parasites showed no noticeable *in vitro* growth defects (not shown). Western blot analysis using the anti-protein C antibody revealed that PfGCN5::PTP was expressed in all developmental stages of the IDC with the peak protein level in early trophozoites (**S1D Fig**). Six protein bands were detected, and the band pattern agreed with that detected with an antibody against the PfGCN5 C-terminal fragment [60], confirming proteolytic processing of PfGCN5 (**S1D Fig**). Live-cell imaging of the green fluorescent protein (GFP)-tagged PfGCN5 parasite line [67] showed that the PfGCN5::GFP protein was expressed throughout the IDC and localized in the nucleus (**S1E Fig**). Thus, we performed the TAP procedure using nuclear extracts from 10^9 synchronized trophozoites of the PfGCN5::PTP parasite, which was followed by liquid chromatography and tandem mass spectrometry (LC-MS/MS) for accurate protein identification. The MS data were subjected to Significance Analysis of INTeractome (SAINT) using a threshold of probability above 94% and false discovery rate (FDR) below 1% [68].

Three independent experiments of TAP and LC-MS/MS consistently identified nine proteins (**Fig 1A** and **S1A and S1B Table**), presumably representing the core subunits of this PfGCN5 complex (**Fig 1A**). This is in sharp contrast to the detection of only some abundant cellular proteins in the three replicates of the wild-type (WT) 3D7 control pulldown experiments (**S1A Table**). Seven proteins identified using the TAP procedure were also present in the PfGCN5-associated proteins identified by a single-step pulldown procedure [62]. In agreement with our earlier work showing interactions between PfGCN5 and PfADA2 [63], these two proteins were among the most enriched proteins in the PfGCN5::PTP pulldown, demonstrating the high efficiency of the TAP procedure and preserved integrity of the complex. Consistent with the recent PfGCN5::GFP pulldown results [62], the PfGCN5 core complex includes two large proteins PfPHD1 (PF3D7_1008100) and PfPHD2 (PF3D7_1433400), each containing four PHD zinc fingers (**Figs 1A, 1B, S2A and S2B**). PfPHD1 also contains two AT hooks, which are DNA-binding domains with a preference for AT-rich regions [69]. Sequence analysis indicated that these PHDs belong to the PHD superfamily with some containing
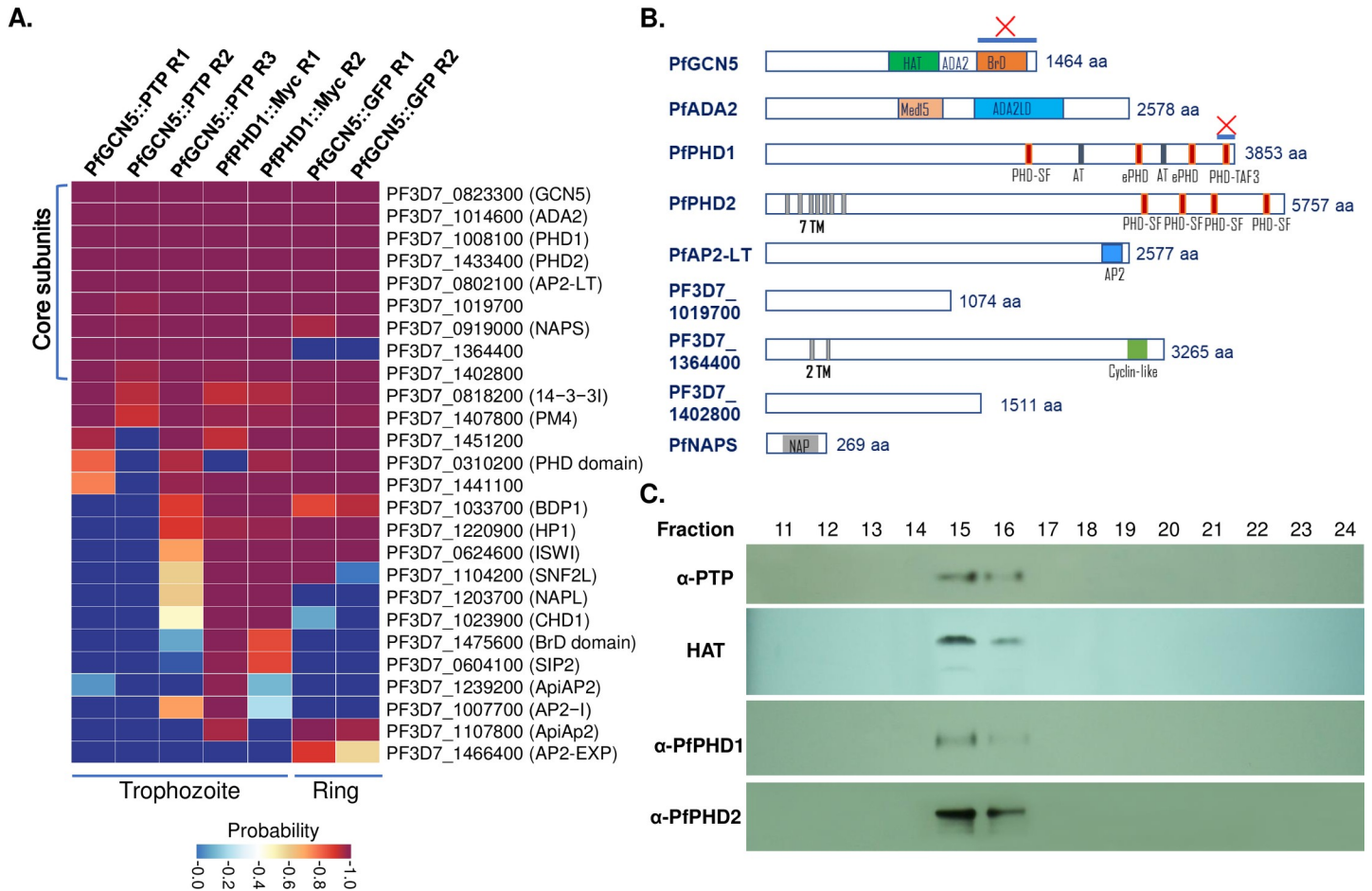
Fig 1. Identification of the PfGCN5 Core Complex in *P. falciparum*. (A) Proteins identified from parasite nuclear extracts by IP and by LC-MS/MS. TAP procedure was performed using the PfGCN5::PTP line at the trophozoite stage (three replicates R1 –R3), while single-step IPs with the anti-Myc and anti-GFP beads were done using the PfPHD1::Myc parasite line at the trophozoite stage and PfGCN5::GFP at the ring stage (two replicates, R1, and R2). The wildtype 3D7 was used as IP control. The wildtype 3D7 was used as IP control. The proteomic data were analyzed by SAINT using a threshold of probability >94% and 1% FDR. Nine proteins consistently identified are marked as the PfGCN5 complex core subunits. Gene ID and annotation are shown on the right. (B) Schematic diagrams showing the features (putative domains and protein size) of the core subunits. HAT: histone acetyltransferase enzymatic domain; ADA2: ADA2 binding domain; BrD: Bromodomain; Med15: Med15 domain; ADA2LD: ASA2-like domain; PHD-SF: PHD finger superfamily; ePHD: extended PHD finger; PHD-TAF3: PHD finger homologous to transcription initiation factor TFIID subunit 3 (TAF3); AT: AT hook; TM: transmembrane region; AP2: AP2-domain; cyclin-like: cyclin-like domain; NAP: nucleosome assembly protein. The C-terminals of PfGCN5 and PfPHD1 labeled by the blue line and "X" containing BrD and PHD-TAF3 were deleted for functional studies (see details in S6 Fig). (C) Gel filtration analysis of the PfGCN5 complex. Aliquots of different fractions were used for Western blots with anti-PTP, PfPHD1 and PfPHD2 antibodies to detect full-length of PfGCN5, PfPHD1 and PfPHD2, and for the HAT assay using recombinant histone H3.

additional cysteine and histidine residues (called extended PHD, ePHD). The ePHD has been found to bind dsDNA, methylated H3K4, or other TFs [70–73]. Only the fourth PHD in PfPHD1 conforms to the canonical PHDs that bind to H3K4me3/2 [74] (**S2C Fig**). Our recent study confirmed that this domain indeed preferentially binds H3K4me3/2 [62]. Furthermore, these two proteins were found to harbor large numbers of acetylation sites in our acetylome study [75], indicating that they are substrates of protein lysine acetyltransferases. An AP2-domain family TF (PF3D7_0802100), named PfAP2-LT, which is highly expressed at the late stages of the IDC [33], was consistently identified in all experimental replicates of the pulldown studies. Of note, the interaction between the PfGCN5 N-terminal fragment and AP2-LT has been identified in a genome-wide yeast two-hybrid screen [76]. Further, a histone assembly protein PfNAPS (PF3D7_0919000) was also identified in the PfGCN5 interactome. Finally, in

the PfGCN5 core complex are three proteins with unknown functions (PF3D7_1019700, PF3D7_1364400, and PF3D7_1402800), which are conserved in all *Plasmodium* species (**Fig 1A and 1B**).

To confirm that PfPHD1 and PfPHD2 are the core constituents of the PfGCN5 complex, rabbit polyclonal antibodies were generated against peptides of PfPHD1 (aa 3685–3702) and PfPHD2 (aa 5738–5756). Indirect immunofluorescence assay (IFA) showed that the pre-immune sera did not react with parasitized red blood cells (RBCs), whereas the anti-PfPHD1 and -PfPHD2 antibodies detected fluorescent signals in the parasite nuclei (**S3A Fig**). Nuclear extracts of trophozoites from the PfGCN5::PTP line were subjected to immunoprecipitation (IP) with anti-PfPHD1 and anti-PfPHD2 antibodies, and the immunoprecipitated proteins were analyzed by immunoblotting with the anti-protein C antibodies. In contrast to the control IP with the pre-immune sera, PfGCN5-PTP was only detected in the IP with the anti-PfPHD1 or -PfPHD2 anti-bodies, confirming co-purification of PfGCN5 with PfPHD1 and PfPHD2 (**S3B Fig**).

Previous IPs and proteomic analysis with the tagged PfPHD1 and PfPHD2 subunits suggest they may be present in different versions of the PfGCN5 complex [62]. Whereas IP from PfPHD1::3×HA only purified PfPHD1, PfGCN5, ADA2, and PF3D7_1402800, IP from PfPHD2::GFP identified 12 putative subunits with marginal enrichment of PfPHD1 but no pulldown of PF3D7_1402800 [62]. To clarify this discrepancy with our TAP results, we sepa-rately tagged two subunits in these two putative versions of the PfGCN5 complexes for recipro-cal IP: the PfPHD1 with a C-terminal c-Myc tag (**S4 Fig**) and PF3D7_1019700 with a C-terminal GFP tag (**S5 Fig**). Correct integration of the *c-Myc* tag at the *PfPHD1* locus and the *GFP* tag at the *PF3D7_1019700* locus was confirmed by Southern blot analysis and integra-tion-specific PCR, respectively (**S4A, S4B, S5A and S5B Figs**). Nuclear localization of the PfPHD1::Myc and PF3D7_1019700::GFP proteins was verified by cellular fractionation–West-ern blot (**S4C Fig**) and live-cell image analysis (**S5C Fig**), respectively. Affinity purification of the trophozoite nuclear extracts from the PfPHD1::Myc parasites with the Myc-trap beads fol-lowed by LC-MS/MS consistently identified all 9 subunits of the putative PfGCN5 complex, including PfPHD2 (**Fig 1A and S1C and S1D Table**). Similarly, two IP replicates from the PF3D7_1019700::GFP identified 7 of the 9 core components of the PfGCN5 complex, includ-ing both PfPHD1 and PfPHD2 (**S5D Fig and S1E and S1F Table**). Furthermore, reciprocal IP using agarose conjugated with anti-PfPHD1 antibodies identified PfPHD2 in the pulldown and vice versa (**S3C Fig**). These results are consistent with the presence of both PfPHD1 and PfPHD2 in the same PfGCN5 complex.

To estimate the size of the PfGCN5 complex, the purified native complex by TAP from the PfGCN5::PTP parasites was subjected to gel filtration, and fractions were assayed for HAT activity and Western blots using anti-PTP, -PfPHD1, and -PfPHD2 antibodies (**Fig 1C**). The results showed that PfGCN5 and its associated HAT activity, PfPHD1, and PfPHD2 all were detected in fractions 15 and 16, which is compatible with one major PfGCN5 complex in *P. fal-ciparum* asexual stages. Based on the calibration using molecular mass standards, the size of the complex was approximately 2.3 MDa, which is comparable to the size (2.26 MDa) esti-mated based on the predicted molecular masses of the 9 core subunits, each presented as a sin-gle copy (**Fig 1B**). Notably, IPs performed using single beads from the PfPHD1::Myc and PF3D7_1019700::GFP parasite lines identified additional proteins associated with chromatin besides the core subunits of the PfGCN5 complex identified by TAP. These proteins include the bromodomain protein 1 (BDP1) [77,78], HP1 [35,44,45], and other AP2 family TFs (**Fig 1A and S1 Table**), suggesting that the PfGCN5 complex may have broader functions in chro-matin biology in the malaria parasite.

The identification of AP2-LT in the core PfGCN5 complex and the presence of other AP2 family members in the IPs suggest that different AP2 TFs may be dynamically associated with

the PfGCN5 complex during development, especially since the IP was conducted at the trophozoite stage when AP2-LT was highly expressed. To investigate this possibility, we performed IPs at the ring stage of PfGCN5::GFP parasite with the GFP-trap beads. Except for PF3D7_1364400, the rest of the eight-core subunits of the PfGCN5 complex were identified, suggesting that AP2-LT is a stable core subunit during the asexual development (**Fig 1A** and **S1G and S1H Table**).

Domain deletions in PfGCN5 and PfPHD1 cause severe growth defects in parasites

To characterize the function of the PfGCN5 complex in transcription regulation, we attempted to knock out the *PfGCN5*, *PfADA2*, *PfPHD1*, and *PfPHD2* genes by double-crossover homologous recombination but were unsuccessful after multiple tries, indicating these genes are essential for parasite survival. This result is consistent with the mutagenesis scores in the genome-wide *piggyback* transposon mutagenesis study showing the essentiality of these genes [79]. Since PTM-binding domains such as the bromodomain (BrD) and PHD are important for anchoring and holding the respective proteins or complexes to the chromatin, we speculated that deleting these domains might disturb histone modifications without causing lethality to the parasite. Thus, we attempted to delete the BrD and PHD from the C-termini of PfGCN5 and PfPHD1, respectively, using a single-crossover gene disruption strategy, and meanwhile tag the C-termini of these truncated proteins with a GFP tag for sorting parasites with truncated PfGCN5 or PfPHD1 (**S6A and S6C Fig**). After transfection, the parasites were selected with WR99210, and GFP-positive parasites were cloned by sorting GFP-positive parasites using flow cytometry. Correct integration of the plasmids at the *PfGCN5* and the *PfPHD1* loci in the parasite genome was confirmed by Southern (**S6B and S6D Fig**) and Western blots (**S6E Fig**). Phenotypic analyses of the parasites with the domain deletions in these two proteins revealed that the parasites with PfGCN5 BrD deletion (GCN5-ΔBrD) and parasites with PfPHD1 PHD domain deletion (PHD1-ΔPHD), to the greatest extent, phenocopied each other (**Fig 2**). Both the GCN5-ΔBrD and PHD1-ΔPHD parasites grew significantly more slowly than the WT parasites; When starting at 0.1% parasitemia, they only reached ~1% parasitemia on day 7 compared to ~10% in WT parasites (**Fig 2A**). Both the GCN5-ΔBrD and PHD1-ΔPHD parasites had a ~2-fold proliferation rate compared to ~5-fold in the WT parasite. A more detailed analysis of the growth defects in these domain deletion lines showed that mature schizonts in these mutant parasites produced similar numbers of merozoites as the WT parasites (**Fig 2B**), but these merozoites had substantially reduced efficiency (by almost 60%) in the invasion of RBCs ($P < 0.05$, paired Wilcoxon test; **Fig 2C**). In addition, these domain deletion mutants also had a 2–3 h longer IDC than the WT parasites ($P < 0.05$, paired Wilcoxon test; **Fig 2D**), and a more extended ring stage (**Figs 2E, 2F and S6F**). Furthermore, these domain deletion parasites were inclined to produce more gametocytes than WT when the gametocytogenesis was induced by using the established method [80] ($P < 0.05$, paired Wilcoxon test; **Fig 2G**).

Domain deletions in PfGCN5 and PfPHD1 are associated with globally reduced H3K9ac and H3K4me3

P. falciparum has an extensively euchromatic epigenome with a preponderance of the histone marks H3K9ac and H3K4me3 [36,54]. The presence of BrD and PHD in the PfGCN5 complex, which bind to acetylated H3K9/14 and H3K4me3/2 marks, respectively, strongly suggests that both domains may be required for anchoring the PfGCN5 complex to chromosomal regions to reinforce the euchromatic state. To determine the impacts of BrD and PHD deletions on
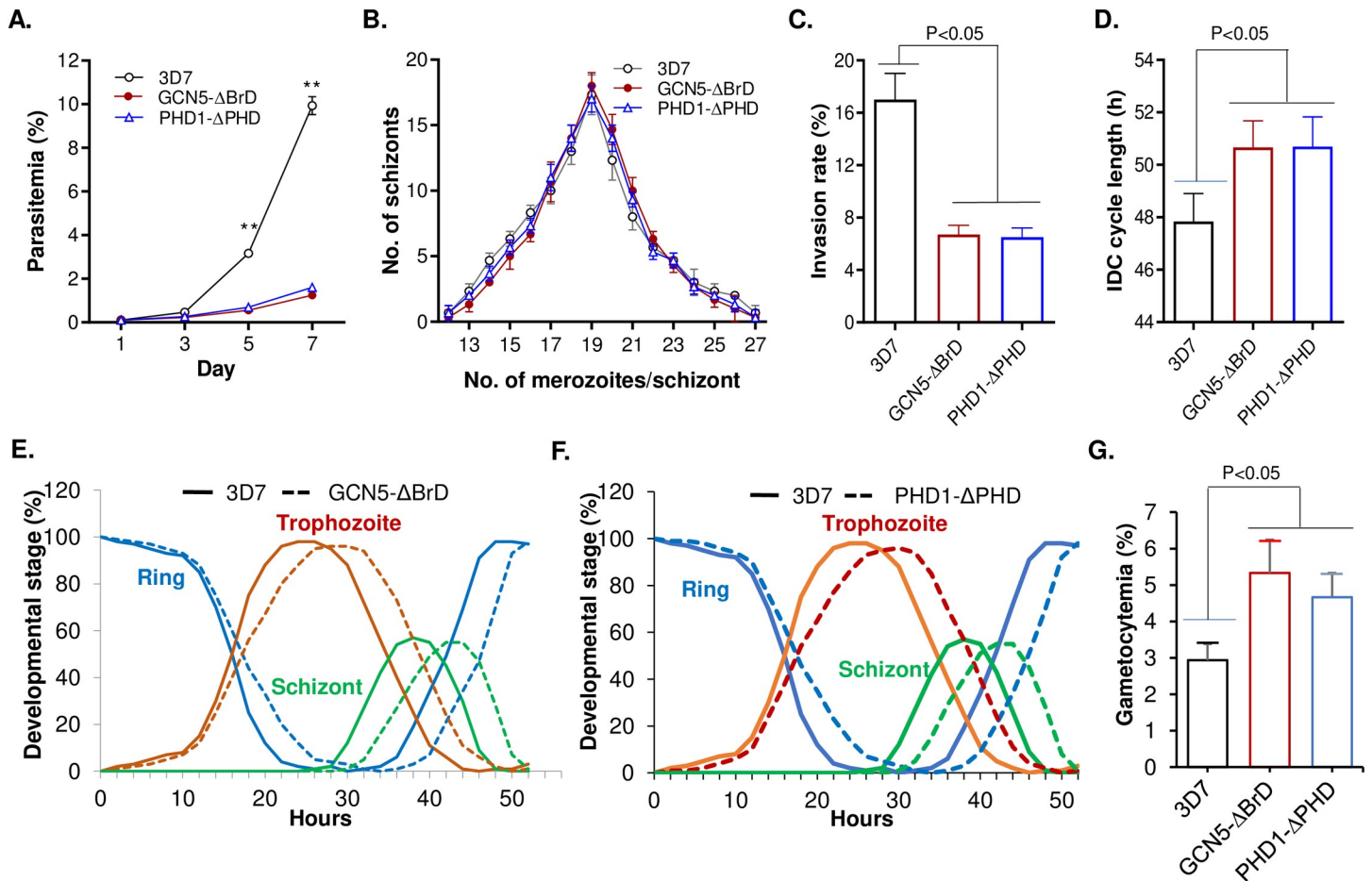
Fig 2. Growth phenotypes in PfGCN5 and PfPHD1 domain deletion mutants. (A) Asexual growth rates of WT 3D7, PfGCN5-ΔBrD::GFP, and PfPHD1-ΔPHD::GFP. ** indicate $P < 0.01$ (ANOVA) at days 5 and 7. The starting parasitemia was 0.1%. (B) The distribution of the number of mature schizonts with a variable number of merozoite. No differences were identified among the three parasite lines ($P > 0.05$, ANOVA). (C) Invasion rates of the GCN5-ΔBrD::GFP and PHD1-ΔPHD::GFP parasite lines estimated by incubating purified schizonts with RBCs ($P < 0.05$, paired Wilcoxon test). (D) The duration of the IDC showing significantly increased lengths in GCN5-ΔBrD::GFP and PHD1-ΔPHD::GFP parasite lines ($P < 0.05$, paired Wilcoxon test). (E, F) Detailed analysis of the IDC showing extended ring stage in the GCN5-ΔBrD::GFP (E) and PHD1-ΔPHD::GFP (F). (G) Gametocytemias at day 6 after induction of gametocytogenesis showing significantly increased gametocytemia in the two domain deletion mutants ($P < 0.05$, paired Wilcoxon test).

https://doi.org/10.1371/journal.ppat.1009351.g002

the overall euchromatic histone marks, histones were purified from parasites of different developmental stages, and several histone marks were analyzed by Western blots. Consistent with PfGCN5 being the major HAT mediating H3K9 and H3K14 acetylation, deletion of BrD in PfGCN5 led to a significant reduction of the H3K9ac and H3K14ac levels in the trophozoite stage, corresponding to the time of peak PfGCN5 expression (**Fig 3A**). Similarly, deletion of the PHD in PfPHD1 also resulted in the reduction of H3K9 and H3K14 acetylation. In comparison, domain deletions in PfGCN5 and PfPHD1 did not cause noticeable changes in H4 tetra-acetylation (at positions H4K5, 8, 14, and 20), which is mediated by another HAT protein, PfMYST [57]. Interestingly, domain deletions in these two subunits of the PfGCN5 complex also resulted in significantly reduced levels of H3K4me3 in trophozoites (**Fig 3A**), another major euchromatin mark conferred by the PfSET1 histone methyltransferase, highlighting the presence of extensive crosstalk between the two euchromatin marks. This result echoes the findings from studies of the SAGA complexes in model organisms, where GCN5 deletion or the Sgf29 Tudor domain deletion reduced the levels of both H3K9ac and H3K4me3 [17,18,81].
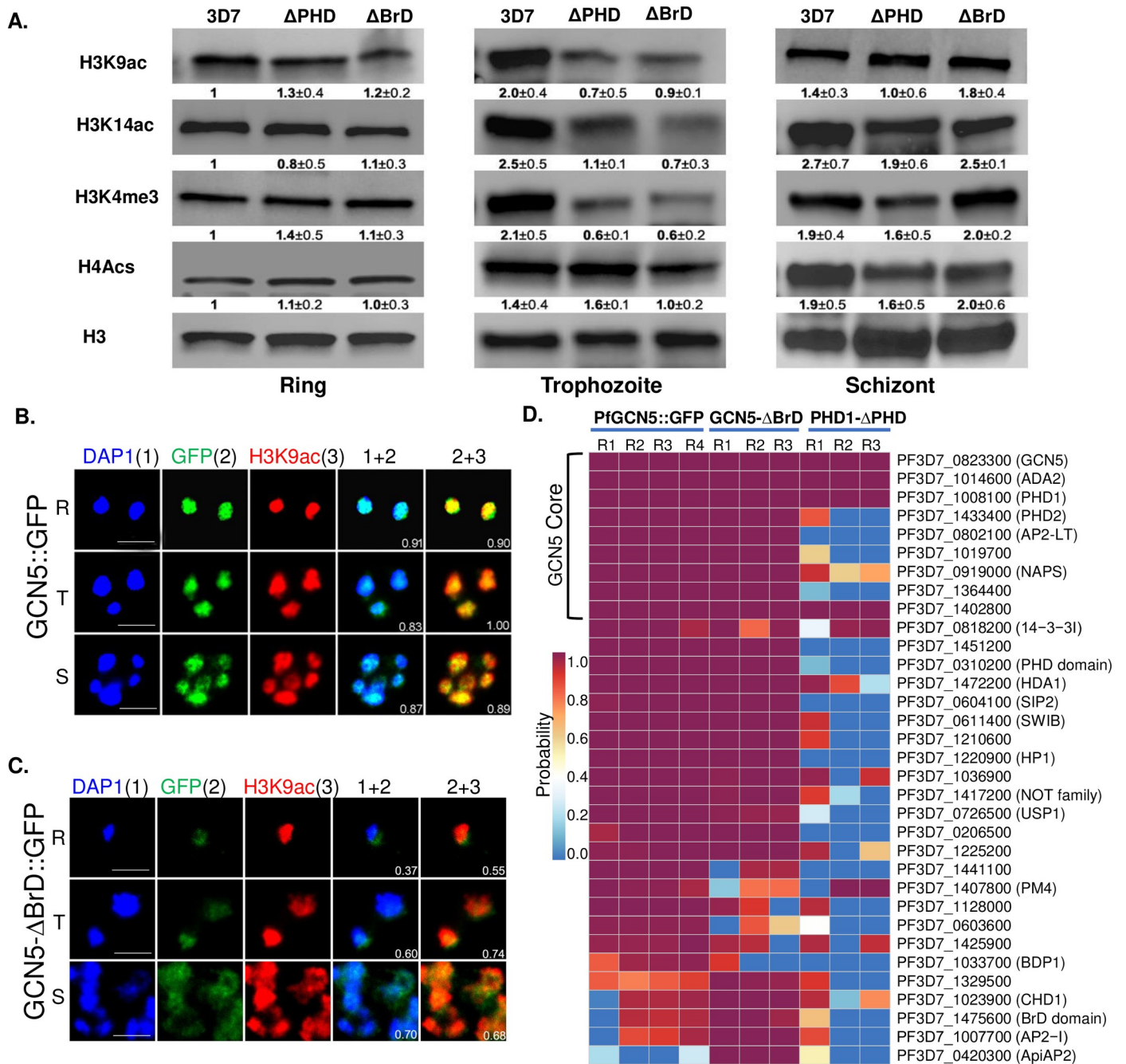
Fig 3. Domain deletions affect the abundance and localization of active histone marks and the integrity of the PfGCN5 complex. (A) The levels of active histone marks in 3D7, PfGCN5-ΔBrD::GFP (ΔBrD), and PfPHD1-ΔPHD::GFP (ΔPHD) parasite lines. Histones were purified from the ring, trophozoite, and schizont stages, and detected by Western blots with specific antibodies against the modified histones H3K9ac, H3K14ac, H3K4me3, and H4Acs. Anti-H3 antibodies were used for loading control. The Western blots were performed in three biological replicates, and the band intensities were determined using a densitometer. The number underneath each band indicates the fold change ± standard deviation between the ratio of the corresponding histone mark normalized to the H3 control. The ratios in 3D7 at the ring stage were set as 1. (B, C) Co-localization of full-length PfGCN5 (GCN5::GFP) (B) or truncated PfGCN5 (GCN5-ΔBrd::GFP) (C) with H3K9ac and DAPI by IFA with anti-GFP and H3K9Ac antibodies. Note the expansion of the truncated PfGCN5-ΔBrD::GFP and H3K9ac beyond the periphery of the euchromatin areas demarcated by DAPI staining. (D) Effects of domain deletions in PfGCN5 and PfPHD1 on complex integrity. Proteins were pulled down from the trophozoite nuclear extracts of the PfGCN5::GFP, GCN5-ΔBrD::GFP, and PHD1-ΔPHD::GFP parasite lines and identified by LC-MS/MS. R1, R2, R3 and R4 indicate individual repeats of the experiment. Shown here are proteins passing the threshold of SAINT (probability >94% and FDR <1%). The nine PfGCN5 complex core subunits were all detected in the IPs of PfGCN5::GFP and GCN5-ΔBrD::GFP, whereas only four of the core subunits were identified in the IPs of PHD1-ΔPHD::GFP.

Taken together, these results indicate that both BrD in PfGCN5 and PHD in PfPHD1 are important for anchoring the PfGCN5 complex to maintain the euchromatic histone marks.

Spatial compartmentalization of chromatin in the nucleus is critical for gene regulation in malaria parasites. The active chromatin marks H3K9ac and the H3K14ac overlap extensively with the DAPI staining (often used to define the euchromatin domains), whereas the hetero-chromatin mark H3K9me3 mostly occupies the nuclear periphery outside of DAPI [35,82]. To analyze whether these changes in histone modifications were associated with altered spatial organization of the chromatin, we used IFA and live-cell microscopy to observe the nuclear loca-tions of these histone modifications as well as the truncated PfGCN5 and PfPHD1. In the PfGCN5-ΔBrD::GFP parasites, Western blot with the anti-GFP antibodies detected reduced expression of the truncated PfGCN5 protein, while the pattern of the PfGCN5 fragments remained similar (S8A Fig). Live-cell microscopy of the GFP-tagged truncated PfGCN5-ΔBrD:: GFP and PfPHD1-ΔPHD::GFP parasites showed that the GFP signals while overlapping largely with the parasite nuclei from DAPI staining (S6G and S6H Fig), were more diffuse than those in the WT parasites (S1E Fig). Consistent results were obtained by IFA with anti-GFP and H3K9ac antibodies in WT and PfGCN5-ΔBrD::GFP parasites (Fig 3B and 3C). In the PfGCN5:: GFP parasites, there were high levels of colocalizations between the DAPI and PfGCN5 (r^2 = 0.83–0.91), and between PfGCN5 and H3K9ac (r^2 = 0.89–1.0), indicating that PfGCN5 is tightly associated with H3K9ac in the active euchromatin area demarcated by DAPI staining (Fig 3B). However, the levels of the colocalization substantially decreased in the PfGCN5-ΔBrD::GFP par-asites (r^2 = 0.37–0.74) (Fig 3C). Some signals of the truncated PfGCN5 were localized beyond the DAPI area, suggesting that PfGCN5 might have spread to the perinuclear heterochromatic area. A similar pattern was found in the PfPHD1-ΔPHD::GFP parasites (S7A and S7B Fig). Since the reduced H3 acetylation in trophozoites after BrD or PHD domain deletion (Fig 3A) could be due to slower replacement of these histone marks after DNA replication, we compared the abundance of the H3K9ac in trophozoites of these parasite lines with 1N or 2N+ single nucleus. While the H3K9ac signal levels in the 1N trophozoites were similar between the WT and domain deletion parasites, the H3K9ac intensities in the 2N+ trophozoites were significantly lower in GCN5-ΔBrD/PHD1-ΔPHD parasites than the WT (S7C Fig). Collectively, these results indicated that domain deletions in PfGCN5 and PfPHD1 altered the nuclear distribution of the truncated proteins and reduced the levels of euchromatin marks in the parasites.

PHD deletion in PfPHD1 affects the integrity of the PfGCN5 core complex

To determine whether BrD deletion in PfGCN5 and PHD deletion in PfPHD1 affected the integrity of the PfGCN5 complex, we performed IP using the GFP-Trap antibodies with nuclear extracts from the individual domain deletion lines and analyzed the affinity-purified proteins by LC-MS/MS. Four replicates of IP using the PfGCN5::GFP parasites as the positive control consistently detected the core components of the PfGCN5 complex (Fig 3D and S2A and S2B Table). IP with the PfGCN5-ΔBrD::GFP parasites also consistently purified the 9 core subunits of the PfGCN5 complex, suggesting the deletion of the BrD from PfGCN5 did not affect the integrity of the complex (Fig 3D and S2C and S2D Table). However, only four major components of the PfGCN5 complex (PfGCN5, PfADA2, PfPHD1, and PF3D7_1402800) were detected from the PfPHD1-ΔPHD::GFP parasites (Fig 3D and S2E and S2F Table). It is noteworthy that both domain deletions resulted in the disassociation between the PfGCN5 core complex and BDP1, whereas BrD deletion resulted in a tighter association between the PfGCN5 core complex and several chromatin regulators, including chromodomain protein 1 (CHD1) and two AP2 TFs (Figs 1A and 3D), indicating that these domain deletions affected the complex integrity and interactions with other chromatin factors.

## BrD and PHD deletions profoundly affect global transcription

Since GCN5-associated complexes facilitate transcription of target genes by bridging transcriptional activator and the preinitiation complex, deletion of domains from subunits of the complex that interact with histone tails weakens the anchoring and retention of the complex, leading to reduced transcriptional activation of the target genes [81,83,84]. To gain a mechanistic understanding of the PfGCN5 complex in transcriptional regulation, we compared the transcriptomes of the WT parasites and parasites with domain deletions. Parasites were highly synchronized from purified schizonts with a 3 h window, and RNA-seq analysis was performed in three biological replicates during the IDC at 10, 20, 30, and 40 h after RBC invasion in the WT parasites and at 10, 23, 33, and 43 h in the parasites with BrD and PHD deletions to more closely match the developmental stages of the WT and domain-deletion parasites based on comparison of their IDC (**Fig 2E and 2F**). Differential gene expression was analyzed by DESeq2 using a *P*-adjustment value of <0.01 as the threshold of significance. To rule out potential normalization artifact by DESeq2, which assumes that the median expression level between the two conditions is the same, we also used Transcripts Per Kilobase Million (TPM) to normalize the RNA-seq data. The results showed that the differentially expressed genes detected by the two normalization methods were highly congruent (**S3 and S4 Tables**).

Compared to the phaseogram of WT parasites displaying a clear cascade-like gene expression pattern [22], PfGCN5 BrD deletion profoundly disturbed the global transcription pattern, causing 3533 (62.6%) genes to be differentially expressed in at least one of the four IDC time points analyzed (**Fig 4A and S3 and S4 Tables**). Specifically, BrD deletion resulted in the down-regulation of 997, 799, 861, and 902 genes, and up-regulation of 1127, 780, 846, and 368 genes at the ring, early trophozoite, late trophozoite, and schizont stage, respectively (**Figs 4B–4D, S8A and S8B**). Noticeably, the numbers of up- and down-regulated transcripts were comparable at all stages except at the schizont stage, where 2.5-fold more transcripts were down-regulated than up-regulated (**Fig 4D**). In comparison, PHD deletion in PfPHD1 caused a similar but more profound disturbance of gene expression during the IDC, with 3870 (68.6%) transcripts being differentially expressed in at least one of the four stages analyzed (**Fig 4A**), which is congruent with the more substantial disruption of the PfGCN5 complex upon PHD deletion (**Fig 4**). The PfPHD1 PHD deletion resulted in the down-regulation of 872, 1021, 557, and 787 genes, and up-regulation of 1481, 1266, 648, and 1028 genes at the ring, early trophozoite, late trophozoite and schizont stage, respectively (**Figs 4D–4F, S8C and S8D**). Of note, only in late trophozoites did PfPHD1 PHD deletion disturb the expression of fewer genes than PfGCN5 Brd deletion (1205 vs. 1707 genes) (**Fig 4D**).

With both PfGCN5 and PfPHD1 being integral members of the PfGCN5 complex, the global transcription changes resulting from the domain deletions of these two genes were remarkably similar; their transcriptomes showed a significant correlation between the respective stages with correlation coefficients ranging from 0.67 to 0.82 (**S8E Fig**). In addition, 44.1–63.8% of the down-regulated genes in each stage were shared between the two domain deletion strains (**Fig 4G**). In comparison, 36.1–49.2% of the up-regulated genes were shared between the two domain deletion mutants in the ring, early and late trophozoites, but this up-regulated gene repertoire in the two domain deletion strains only shared 18.8% during the schizont stage (**Fig 4H**).

BrD and PHD deletions affect parasite-specific cellular pathways

To determine whether deletion of PfGCN5 BrD or PfPHD1 PHD affected specific biological processes, Gene Set Enrichment Analysis (GSEA) [85,86] and gene ontology (GO) enrichment analysis (PlasmoDB) were performed on the genes with significantly altered expression
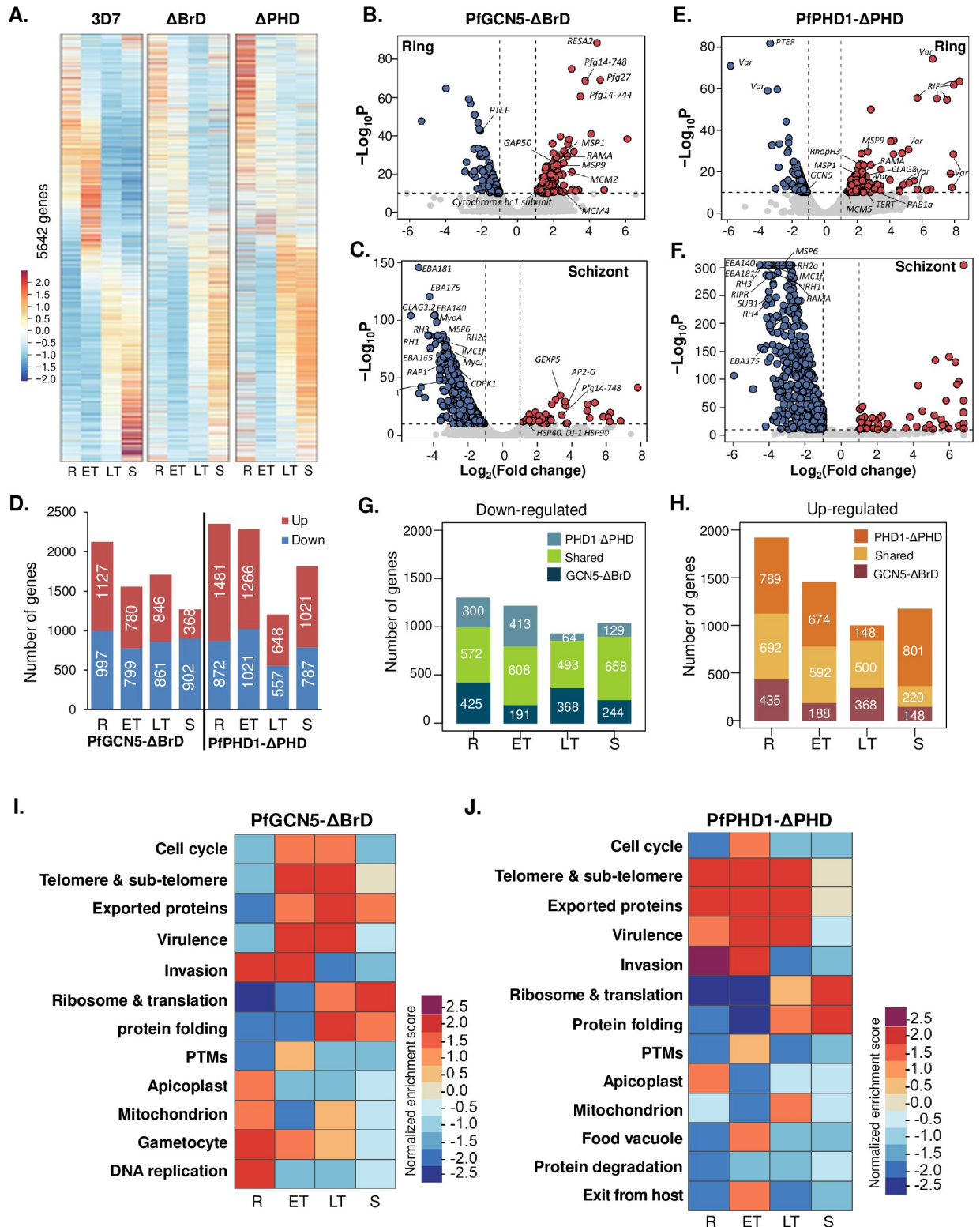
Fig 4. Global transcriptomic changes up domain deletions in PfGCN5 and PfPHD1. (A) The phaseograms of transcriptome from the WT 3D7, PfGCN5-ΔBrD::GFP (ΔBrd), PfPHD1-ΔPHD::GFP (ΔPHD) showing the disturbance of the cascade-like gene expression pattern in the deletion mutants at different developmental stages. R, ring; ET, early trophozoite; LT, late trophozoite; S, schizont. (B, C) Volcano plots showing altered gene expression at the ring (B) and schizont (C) stages in PfGCN5-ΔBrD::GFP compared to the WT 3D7. The x-axis indicates log$_2$ (Fold change) of the transcript level in PfGCN5-ΔBrD::GFP compared to WT 3D7, while the y-axis indicates -log$_{10}$ of the *P* values.(D) Number of

genes with altered expression at different developmental stages of the IDC in the two domain deletion mutants. The up- and down- regulated genes are labeled in red and blue, respectively. (E, F) Volcano plots showing altered gene expression at the ring (E) and schizont (F) stages in PfPHD1-ΔPHD::GFP compared to the WT 3D7. The x-axis indicates $\log_2$ (Fold change) of the transcript level in PfPHD1-ΔPHD::GFP compared to WT 3D7, while the y-axis indicates $\log_{10}$ of the *P* values. (G, H) Overlaps of down-regulated (G) and up-regulated (H) genes between the PfGCN5-ΔBrD::GFP and PfPHD1-ΔPHD::GFP parasite lines at different stages. (I, J) The enriched functions or pathways of up-regulated and down-regulated genes upon PfGCN5 BrD (I) and PfPHD PHD (J) deletion determined by GSEA. Each pixel represents the normalized enrichment score (NES). The positive and negative NESs represent up-and down-regulated functions after domain deletions, respectively.

(**Figs 4I, 4J, S9 and S5 Table**). The two analyses identified similar sets of enriched gene categories during the IDC. During the early IDC stages, transcripts associated with cytoadherence, merozoite invasion, DNA replication, and organellar activities were upregulated. In particular, the 60 *var* genes, encoding the virulent factor PfEMP1 that mediates cytoadherence, were dramatically upregulated in the early stages. At the early trophozoite stage, the overall transcripts of *var* genes in the WT 3D7 were sharply decreased. In contrast, the *var* transcripts remained at high levels in the domain deletion parasites (~4-fold higher upon BrD deletion and ~25-fold higher upon PHD deletion) (**Fig 5A and 5B and S6 Table**). It is noteworthy that many *var* members were upregulated, albeit *var2csa* was a major *var* gene expressed in PfGCN5-ΔBrD, suggesting activation of the overall *var* gene family. Western blots using antibodies against the conserved cytoplasmic ATS domain of the PfEMP1 proteins detected more complicated expression patterns and higher abundance of the PfEMP1 on the surface of RBC infected by trophozoite-stage parasites upon PfGNC5 BrD and PfPHD1 PHD deletions (**Fig 5C and 5D**). To further determine whether domain deletion in PfGCN5 and PfPHD1 activated multiple *var* members in a single infected RBC, we performed single-cell RNA-fluorescent in situ hybridization (FISH) using the Type B *var* exon 2 as the probe [35], which is predicted to hybridize to 22 Type B *var* genes. *Var* genes are clustered into 6–8 foci at the nuclear periphery and colocalized with the "telomere bouquets" [38], while the active *var* gene is localized to a *var*-specific expression site [87,88]. Consistent with the mutually exclusive expression of *var* genes in single cells, the majority of the RNA-FISH positive cells in 3D7 contained one fluorescent spot (mean ± standard deviation, 1.04±0.21, n = 67) indicating expression of one Type B *var* (**Fig 5E**). In contrast, 43.9% and 58.2% positive rings had more than one hybridization signal in the PfGCN5-ΔBrD (1.55±0.66, n = 66) and PfPHD1-ΔPHD parasites (1.91±0.98, n = 79), respectively. In addition, 28.7% (45/157) of the WT 3D7 ring-stage parasites showed hybridization, which increased to 34.5% (61/177) and 41.3% (71/172) in the PfGCN5-ΔBrD and PfPHD1-ΔPHD rings, respectively. It is noteworthy that the hybridization signals were mostly localized in areas at the periphery of the DAPI staining. Thus, these results indicate the presence of multiple *var* expression sites in the PfGCN5-ΔBrD and PfPHD1-ΔPHD parasites.

Conversely, genes involved in the biological processes of translation and transcription were significantly enriched in the down-regulated genes upon BrD or PHD deletion during the early IDC, which was probably responsible for the slowing down of development (**Figs 4I, 4J, S9 and S6 Table**). During the late IDC (late trophozoites and schizonts), genes involved in RBC invasion were greatly reduced, which is consistent with the phenotype of reduced RBC invasion rates of the PfGCN5-ΔBrD and PfPHD1-ΔPHD merozoites (**Figs 4I, 4J, S9 and S6 Table**). Of the 86 putative invasion-related genes [89], 76 showed peak expression at the late stages of IDC in WT parasites (**S10B Fig**). Except for *MSRP1*, which was up-regulated, 75 genes were significantly down-regulated at the late stages in the PfGCN5-ΔBrD and PfPHD1-ΔPHD parasites (**Figs 6A and S10B**). In addition, other enriched gene categories such as "exit from host" and cell cycle were also down-regulated in late IDC (**Figs 4I, 4J and S9**). These data collectively indicate the involvement of the PfGCN5 complex in the regulation of the general

A.

B.

C.

D.

E.
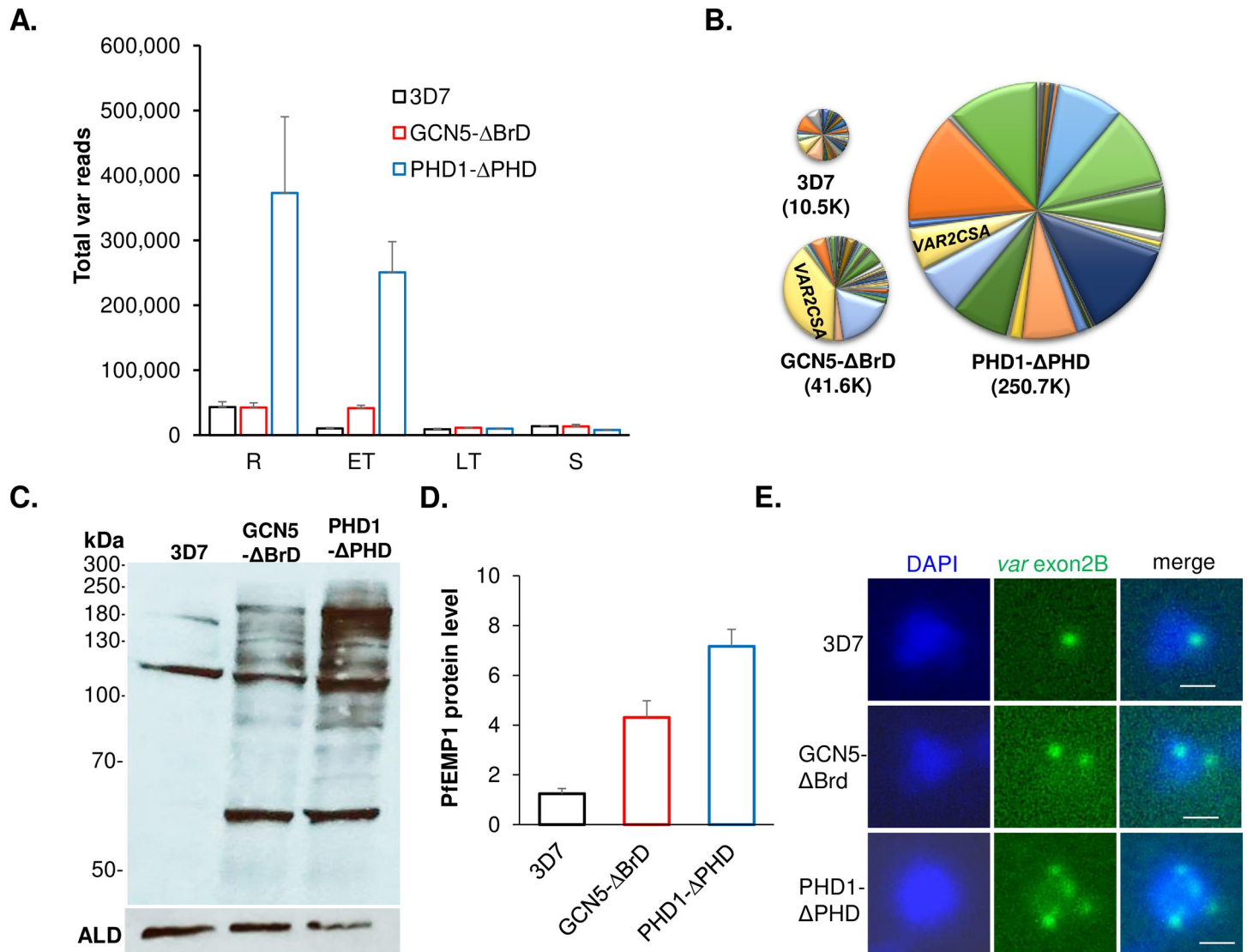
Fig 5. Virulence gene expression altered upon domain deletions. (A) The expression of total *var* genes at different developmental stages. The y-axis indicates the total reads of *var* genes from RNA-seq. R, ring; ET, early trophozoite; LT, late trophozoite; S, schizont. (B) Pie graphs showing the overall levels of the *var* gene transcripts in the WT 3D7, PfGCN5-ΔBrD::GFP, and PfPHD1-ΔPHD::GFP parasite lines at the early trophozoite stage. The numbers in parentheses are the total expression of all *var* genes identified by RNA-seq analysis. (C) Western blot showing PfEMP1 protein levels in the iRBC membranes of the WT 3D7, PfGCN5-ΔBrD::GFP, and PfPHD1-ΔPHD::GFP parasite lines with the anti-ATS antibodies. Aldolase (ALD) expression was used as the loading control. (D) Bar graph showing the overall PfEMP1 protein levels in WT 3D7, PfGCN5-ΔBrD::GFP, and PfPHD1-ΔPHD::GFP parasite lines. Bars indicate means and standard deviations from five replicates. (E) Representative images of RNA FISH analysis showing the single locus of the B-type *var* gene expression in the WT 3D7 and more than one B-type *var* gene locus in the two deletion mutants.

cellular processes such as transcription, translation, and organellar function, as well as parasite-specific processes of pathogenesis and host cell invasion.

Potential coordination of the PfGCN5 complex by AP2 transcription factors and BDP1

The profound effects of PfGCN5 BrD/PfPHD1 PHD deletion on particular pathways such as invasion and cell adhesion suggest that these coordinated changes may involve the participation of specific TFs of the ApiAP2 domain family [90,91]. The consistent pulldown with the PfGCN5 complex of the AP2-LT that is expressed abundantly in late stages of the IDC and
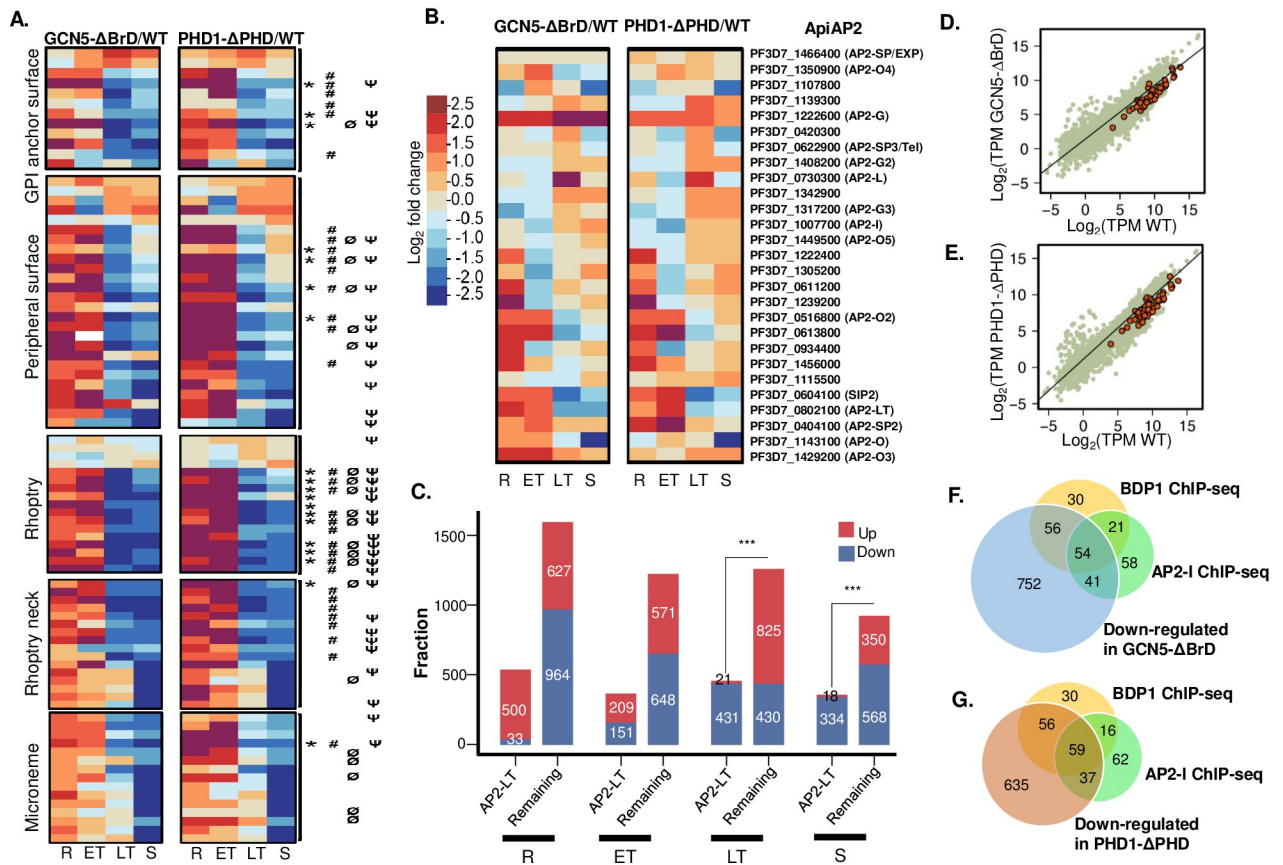
Fig 6. Down-regulation of invasion-related pathway and alteration of AP2 genes in domain deletion mutants. (A) Heatmaps displaying down-regulation of genes involved in the invasion of the RBC in the two deletion mutants. * and # indicate the AP2-I and putative AP2-LT target genes, respectively. Ø and Ψ indicate the down-regulated genes upon knockdown of BDP1 and the target genes identified by BDP1-HA ChIP-seq analysis, respectively. (B) Heatmaps showing altered expression of the AP2 genes in the deletion mutants. (C) Putative AP2-LT target genes (with AP2-LT binding motifs) are significantly enriched in the down-regulated genes in PfGCN5-ΔBrD::GFP at the late stages. The numbers of up- and down-regulated genes upon PfGCN5 BrD domain deletion are shown as the red and blue bars at four developmental stages. These altered genes were further classified as the putative target genes of AP2-LT and the remaining genes. R, ring; ET, early trophozoite; LT, late trophozoite; S, schizont. ***, $P < 0.001$ (Fisher's exact test).

https://doi.org/10.1371/journal.ppat.1009351.g006

occasionally other AP2 proteins (**Figs 1A** and **3D**) [62] suggests coordination of chromatin modification with transcription activators/repressors. To this end, we analyzed the transcriptional changes of all 27 ApiAP2 TFs after BrD or PHD deletion (**Figs 6B and S10C**). Indeed, the cascade of AP2 transcriptions was substantially disturbed; some AP2-TFs such as AP2-SP2 and AP2-O3 were activated at stages when they are normally silenced in WT parasites, whereas some (e.g., AP2-SIP2, AP2-O, AP2-I, and AP2-LT) were down-regulated at the stages when they are supposed to be active (**Figs 6B and S10C and S6 Table**). PfSIP2 is associated with the chromosomal end clusters and is required for heterochromatin formation and genome integrity, including the silencing of subtelomeric *var* genes [92]. Its down-regulation upon BrD and PHD domain deletion may influence the organization of the subtelomeric heterochromatin, resulting in the overall de-repression of *var* genes (**Figs 6B and S10C**). The master regulator of gametocytogenesis AP2-G [93,94] was consistently up-regulated upon Brd and PHD deletions (**Fig 6B**), which agrees with the increased gametocytogenesis detected in the mutant parasite lines (**Fig 2G**). The down-regulation of AP2-I and AP2-LT might partially explain the down-regulation of the invasion-related gene upon domain deletions. Of the 75 invasion-related

genes down-regulated upon BrD or PHD deletion, 19 (mostly associated with the rhoptry) are targets of AP2-I, and 33 were predicted targets of AP2-LT (**Fig 6A** and **S6 Table**) [33,78]. The AP2-LT subunit of the PfGCN5 complex is predicted to bind to 986 genes with the motif sequence ACACA [33]. Analysis of the genes altered upon BrD deletion in PfGCN5 and PHD domain deletion in PfPHD1 revealed that genes down-regulated in late trophozoite and schizont stages were significantly enriched in those containing the AP2-LT binding motif (**Figs 6C and S10D**). This finding is consistent with the decreased recruitment of the PfGCN5 complex in the deletion mutants by AP2-LT to genes with AP2-LT binding motifs, resulting in extensive down-regulation of the gene categories during the late-stage development (**Fig 6B**). In contrast, genes up-regulated at the ring and trophozoite stages were significantly enriched in those containing the AP2-LT binding motif (**Figs 6C and S10D**), in agreement with the up-regulation of AP2-LT at the early stages upon domain deletion (**Fig 6B**). Thus, the unique presence of AP2 TFs in the GCN5 complexes in apicomplexan parasites suggests that the GCN5 complexes are specifically recruited to regulate the expression of certain clusters of genes [11].

The parasites with PfGCN5/PfPHD1 domain deletion displayed a similar invasion phenotype with the BDP1 knockdown parasites [77]. Of the down-regulated invasion genes upon BrD and PHD domain deletions, 24 and 34 are BDP1 targets identified by BDP1 knockdown and BDP1 chromosome immunoprecipitation (ChIP)-seq analysis, respectively (Fig 6A). BDP1 regulates these invasion-related genes by binding to the acetylated H3 at their TSSs. Thus, the disassociation between the PfGCN5 complex and BDP1 upon domain deletions (**Fig 3D**) may underlie such a phenotypic similarity. Additionally, BDP1 knockdown resulted in the down-regulation of 47 genes at the later stage of IDC (TP5) [77] and a significant proportion of these genes were also down-regulated in the two domain deletion mutants at the schizont stage (**Fig 6D and 6E,** p <0.001, Fisher's exact test, compared to the expectation from the whole genome scale). Furthermore, the potential target genes of BDP1 and AP2-I identified by ChIP-seq also showed substantial overlaps with genes down-regulated at the schizont stage upon BrD and PHD domain deletions (**Fig 6F and 6G**). These data highlight the connection between the recruitment of the PfGCN5 complex to specific gene groups by the AP2 domain TFs and the BrD-containing reader complex in orchestrating transcription regulation.

BrD and PHD deletions broadly alter chromatin structure

The above transcriptomic analyses showed that the expression of many genes was disturbed in the PfGNC5-ΔBrD and PfPHD1-ΔPHD parasites; genes that are normally active were down-regulated, whereas genes supposed to be silent were active at the wrong time during the IDC. Since epigenetic regulation of gene expression in *P. falciparum* is most evident in the heterochromatic regions [27], while gene expression from the euchromatic regions correlates positively with the chromatin accessibility [52], we compared the chromatin status and accessibility of genes with altered expression upon PfGCN5 and PfPHD1 domain deletions. We first compared the up- and down-regulated genes with the accessibility of their promoters previously determined using the published assay for transposase accessible chromatin sequencing (ATAC-seq) [52]. Based on the value of ATAC-seq peak in the promoter (chromatin openness level), the down-regulated genes upon BrD or PHD deletion had more open chromatin structure at their promoters in the WT parasites, whereas the up-regulated genes had less open promoters in the WT parasites (**Fig 7A**). Conversely, when the genes with altered expression were compared with the published HP1 occupancy signals, the up-regulated genes upon BrD or PHD deletion are significantly more often associated with the heterochromatin loci that are normally enriched with HP1 and repressed during the IDC [95] (**Fig 7B and**
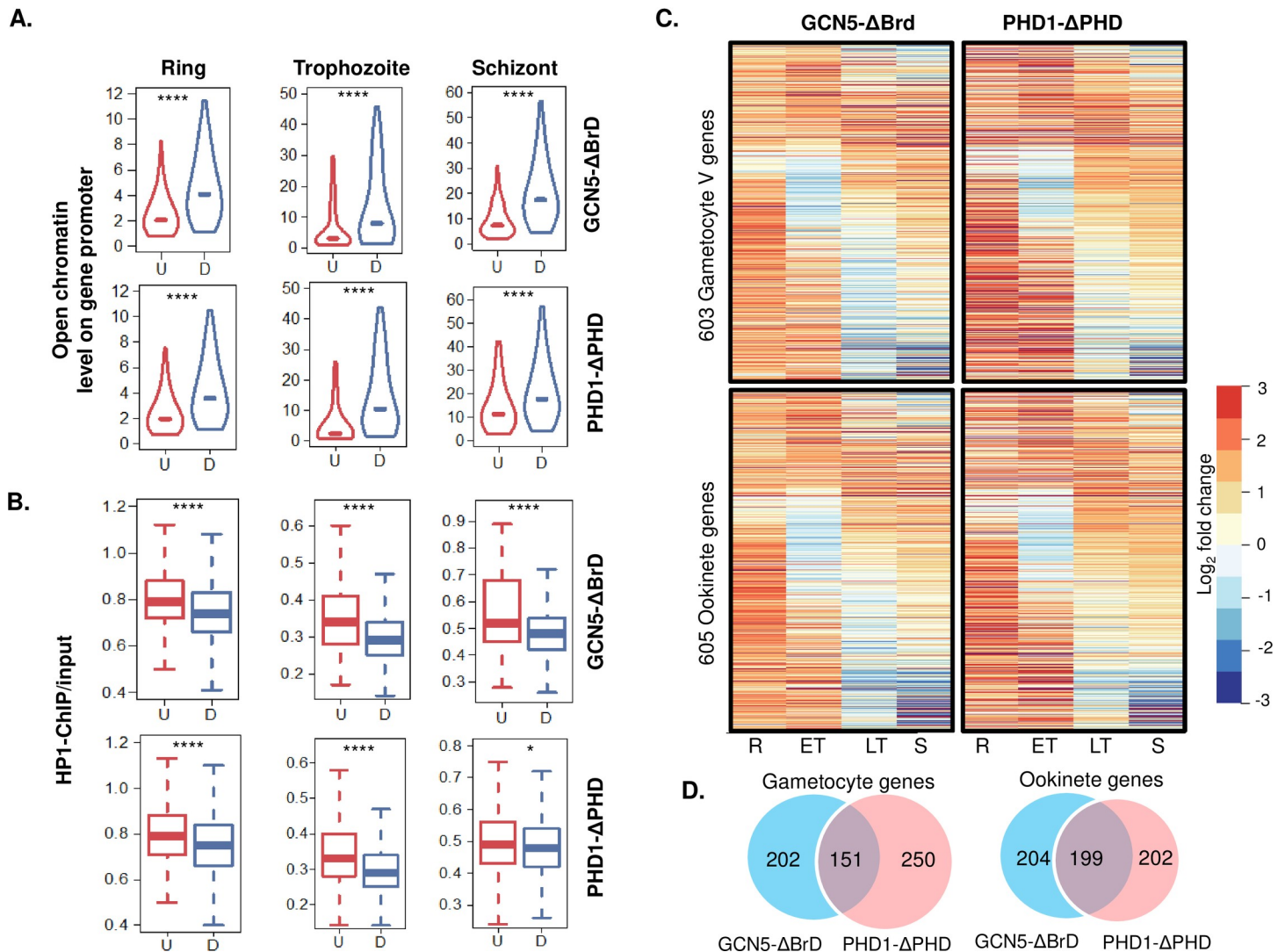
Fig 7. Correlation of genes showing altered expression in domain deletion mutants with promoter accessibility and chromatin states. (A, B) Changed levels of gene expression in PfGCN5-ΔBrd and PfPHD1-ΔPHD are negatively correlated with the accessibility of the promoters (from the ATAC-seq analysis, The y-axis shows that the ratio of ATAC-seq peak (scaled per million reads) vs genomic DNA library) (A), but are positively correlated with the heterochromatin state (represented by the HP1 occupancy) (B). U, upregulation; D, downregulation. *, $P < 0.05$; ****, $P < 0.0001$ (Wilcoxon rank-sum test). (C) Heatmaps displaying the transcriptional activation of gametocyte and ookinete genes in the domain deletion mutants. R, ring; ET, early trophozoite; LT, late trophozoite; S, schizont. (D) Overlaps of activated gametocyte- or ookinete-specific genes between PfGCN5-ΔBrd and PfPHD1-ΔPHD.

S7 Table). This group of genes includes many variant gene families (*var*, *rifin* and *stevor*) and AP2-G (**Figs 5B and 6B and S7 Table**). In addition, genes specific for sexual-stage development, which usually are silent during the IDC, are also among the genes that were up-regulated upon BrD or PHD deletion but have low accessibility in their promoters during the IDC in the WT parasites. BrD deletion led to significant up-regulation of 353 gametocyte- and 401 ookinete-specific genes, respectively (**Figs 7C, 7D, S10E and S8 Table**), and many were up-regulated at the ring stage. Similarly, PHD deletion caused up-regulation of 403 gametocyte- and 401 ookinete-specific genes, respectively (**Figs 7C, 7D, S10E and S8 Table**). Among them, 151 gametocyte- and 199 ookinete-specific genes are shared between both deletional mutants. Taken together, both domain deletions similarly affected chromatin structure and led to the activation of genes involved in sexual development.

To verify that the PfGCN5 complex directly regulated the accessibility and chromatin state of the promoters, we selected three genes to evaluate the recruitment of the complex by ChIP with antibodies against the tags fused to PfGCN5 or PfPHD followed by qPCR analysis, and the results were compared to those with respective control antibodies (**S11 Fig**). Compared to the WT parasites, the truncated PfGCN5-ΔBrD and PfPHD1-ΔPHD were significantly depleted at the *PfMSP1* promoter in schizonts, whereas they were enriched at the ring stage (**S11 Fig**). Their dynamic associations with the *PfMSP1* promoter were correlated with the down- and up-regulation of *PfMSP1* at the schizont and ring stages, respectively, in these two domain deletion lines. Consistently, the PfGCN5-ΔBrD and PfPHD1-ΔPHD proteins were significantly enriched at the promoter of the *var2csa* gene and the gametocyte-specific gene *Pfg27/25* at the ring stage (**S11B and S11C Fig**), which was correlated with significant up-regulation of these two genes in the domain deletion parasites. To determine whether activation of genes located in the heterochromatin after domain deletions were due to the alteration of chromatin states, we selected *VAR2CSA* and a *RIFIN* gene, which were significantly up-regulated in domain deletion mutants at the ring stage, for the evaluation of the H3K9me3 and H3K9ac levels by ChIP-qPCR. In general, domain deletions decreased the heterochromatin mark H3K9me3 at the promoters of these genes, whereas domain deletions elevated the H3K9ac mark (**S12 Fig**).

Discussion

An unusual aspect of the chromatin-mediated gene regulation in the malaria parasite *P. falciparum* is that the parasite epigenome is predominantly euchromatic, marked extensively with H3K9ac and H3K4me3 [36,53], whereas heterochromatin-associated histone modifications H3K9me3 and H3K36me3 are localized to genes undergoing variable expression [35,96]. This is contrasted to most eukaryotes where these heterochromatin marks are found in genes throughout the genome. We identified a unique GCN5 complex in *P. falciparum* responsible for depositing the euchromatic marks H3K9ac and H3K14ac, which differs drastically from the canonical SAGA complex that is conserved from yeast to humans. Functional characterization of two major subunits of the PfGCN5 complex demonstrated its crucial functions in regulating global gene expression and parasite biology during its development in the host RBCs.

The evolutionarily conserved SAGA complex has a modular structure that supports multiple activities including histone acetylation, deubiquitination, and interactions with TFs [9]. In the current study, we defined the subunit structure of the GCN5 complex in *P. falciparum*, using multiple approaches. We discovered that it completely lacks the deubiquitinase, the TBP-associated proteins, and the core structural module with the histone folds. Even for the HAT catalytic core [10], the *P. falciparum* GCN5 complex is also distinctive with the conservation of only the GCN5 and ADA2 homologs. Although both *Plasmodium* and *Toxoplasma* belong to Apicomplexa, the PfGCN5 complex appears to differ substantially from the *T. gondii* GCN5b complex [11,12], as the latter contains additional proteins potentially involved in RNA binding and transcription elongation. In the PfGCN5 complex, the H3K4me3-binding activity, mediated by the tandem tudor domains of Sgf29 in the SAGA complexes [81,97], is replaced by the PfPHD1 protein [62]. Moreover, PfPHD2 in the PfGCN5 complex contains four atypical PHDs, and may bind to other histone modifications. Importantly, since deletion of either BrD or PHD affected their localization and reduced the levels of both H3K9ac and H3K4me3, these domains are needed for anchoring and retention of the PfGCN5 complex on chromatin, similar to what was observed in the SAGA complex [17,18,81]. This result also implies the presence of synergistic crosstalk between the PfGCN5 complex and the histone H3K4me3 methyltransferase complex. As in model organisms, the binding of GCN5 BrD to H3K9ac

likely promotes H3 acetylation, which in return augments H3K4me3, since histone methyl-transferases have a preference for the acetylated H3 tail [98–101]. The interactions between PfGCN5 and PfSET1 identified through yeast two-hybrid analysis further attests to the cross-talk between these euchromatic histone marks [76]. Given that the H3K4me3 levels are gradually increased toward the late stages of the IDC [54] and that most genes affected during PfSET1 knockdown are also expressed at the late stages [59], the intricate interplay between the writer complexes of these euchromatin marks needs to be further dissected.

Our earlier suggestion that PfPHD1 and PfPHD2 may represent different versions of the PfGCN5 complex was based on the identification of only four proteins (PfGCN5, PfADA2, PfPHD1 and PF3D7_1402800) in the PfPHD1::3×HA pulldown and a complete lack of PF3D7_1402800 from the PfPHD2::GFP pulldown [62]. Here we provided evidence suggesting that both PfPHD1 and PfPHD2 are subunits of the same PfGCN5 complex. First, reciprocal pulldown with both the PfPHD1::Myc and PF3D7_1019700::GFP, which belong to the two putative PfGCN5 subcomplexes suggested earlier, identified the core components of the PfGCN5 complex with the abundant presence of both PfPHD1 and PfPHD2 (**Fig 1** and **S1 Table** Additionally, the anti-PfPHD1 antibodies co-IPed PfPHD2 and vice versa. Second, PfPHD1 and PfPHD2 were co-eluted in the same fractions during gel filtration of the PfGCN5 complex. Third, the predicted size of the single PfGCN5 complex is compatible with the summation of the single-copy core subunits, while missing either of these two large PHD proteins would drastically reduce the size of the complex. Thus, this discrepancy may be due to the use of different tags for PfPHD1 (c-Myc vs. 3×HA tag) and the different stringency of the analysis (1% FDR used here vs. 10% used earlier). Also, we found that PfPHD1 could not be tagged with a larger tag such as the GFP (not shown), suggesting that tagging PfPHD1 with 3×HA may interfere with the integrity of the PfGCN5 complex. Interestingly, pulldowns with both PfPHD1::3×HA and PfPHD1-ΔPHD::GFP identified the same four subunits of the PfGCN5 complex (**Fig 3D**). Thus, studies employing biochemical and cryogenic electron microscopy will allow a further resolution of the PfGCN5 complex.

The SAGA co-activator complex plays a critical role in regulating global gene expression [17,18]. In *P. falciparum* with an unusual, dominantly euchromatic epigenome, the significance of the PfGCN5 complex is demonstrated by the essence of several core subunits for asexual development. Although domain deletion partially relieved the problem of lethality, deletion of either the BrD in PfGCN5 or PHD in PfPHD1 caused considerable growth defects during the IDC and altered expression of >60% of genes with an approximately equal number of up- and down-regulated genes. This defective gene expression pattern may be due to reduced levels of H3K9ac and H3K4me3, as well as mislocalization of the PfGCN5 complex. This may have led to the opposite changes in chromatin state, which are correlated with the genome-wide changes in the expression pattern. These global transcriptional changes are reminiscent of those occurring when parasites were treated with the histone deacetylase inhibitor apicidin, which caused a reduction of H3K9Ac and H3K4me3 [102]. Analysis of genes with altered expression upon domain deletions for their chromatin state (HP1 occupancy) and promoter openness (ATAC-seq) provided indirect evidence supporting the mislocalization of the PfGCN5 complex in the deletion mutants. It is also noteworthy that PHD deletion in PfPHD1 caused more severe effects on gene expression, which can be explained by the disturbance of the integrity of the PfGCN5 complex upon PHD deletion, suggesting that PfPHD1 may play a scaffolding role for the structural integrity of the complex. Interestingly, the transcriptomic changes after BrD and PHD domain deletions (presumably due to reduced expression and mislocalization effects) are distinct from those after deletion of the SAGA subunits in yeast and human cells, which showed global down-regulation of transcription [17,18].

SAGA is recruited to the promoters through the interactions between Tra1 and TFs. Although a Tra1 homolog is present in the *P. falciparum* genome, it was not identified in the PfGCN5 complex. Another distinguishing feature of the PfGCN5 complex is the presence of an AP2-domain TF (PfAP2-LT) as a consistent member of the complex. Of note, the core GCN5b complex in the *T. gondii* tachyzoites also contains multiple AP2 factors [11], suggesting a conserved characteristic in these lower-branching eukaryotes. These TFs would allow direct recruitment of the GCN5 complex to the target gene promoters, circumventing the need for a bridging factor such as Tra1. In addition to the identification of AP2-LT in the complex, two other AP2 factors (AP2-I and PF3D7_1239200) were also identified in the PfPHD1::Myc pulldown at the trophozoite stage, suggesting that they might be either loosely associated with the GCN5 complex or represent additional variations of the minor GCN5 complexes. In support of this notion, PfGCN5 was also identified in the AP2-I pulldown [78]. The pulldown from PfGCN5::GFP at the ring stage identified almost all PfGCN5 subunits, indicating that AP2-LT is a relatively consistent subunit of the PfGCN5 complex. Furthermore, two other AP2 factors (AP2-EXP and PF3D7_1107800) were also found in the PfGCN5::GFP pulldown. With the H3K9ac mark at the promoter regions dynamically following the pattern and level of transcription throughout the IDC [54], it is logical to propose that the dynamic recruitment of the PfGCN5 complex to different promoters is mediated by different AP2 factors. This hypothesis is compatible with the recruitment of the GCN5 complex by AP2-I to the promoters of invasion-related genes to acetylate the histones, which then recruit the BrD protein PfBDP1 [78]. In line with this, the genes predicted to be the targets of AP2-LT were mostly down-regulated upon PfGCN5 BrD and PfPHD1 PHD deletions, consistent with the AP2-LT-mediated recruitment of the PfGCN5 complex to the promoters of these genes. Of the 86 invasion-related genes expressed in merozoites, 33 were predicted to be the AP2-LT target genes, and 19/34 of these genes also are AP2-I/DBP1 targets by ChIP-seq analysis (**Fig 6A**). Moreover, the majority of those AP2-LT target genes specifically affected by the domain deletions in PfGCN5 and PfPHD1 are expressed in late stages, coincident with the peak expression of the AP2-LT (**Fig 6C**).

Antigenic variation in *P. falciparum* is mediated by the monoallelic expression of the ~60 members of the *var* gene family [103]. *Var* gene clusters are located in the heterochromatin regions of the nuclear periphery and their expression is associated with the relocation and change of the promoter to a euchromatic state [42,87,104]. Such a mutually exclusive, monoallelic expression pattern of *var* genes is completely disrupted when the PfGCN5 BrD or PfPHD1 PHD domain was deleted, evidenced by the simultaneous expression of multiple *var* genes in single infected RBCs. This phenotype is similar to what was observed when the histone deacetylate PfHda2, PfSir2A, B, and the heterochromatin marker PfHP1 were experimentally knocked out or knocked down [46,105–107]. Given the presence of potential binding elements for AP2 factors in the *var* promoters and the fact that the expression of many AP2 TFs was disturbed after domain deletion, such as down-regulation of PfSIP2, we cannot fully exclude the possibility that the activation of the *var* gene family upon PfGCN5 or PfPHD1 domain deletion may be due to altered recruitment of the PfGCN5 to *var* promoters through AP2 factors present in subsets of the GCN5 complex. However, the increased expression of most genes located in the heterochromatin regions marked by PfHP1 suggests that the expression of the whole *var* gene family may reflect a general loss of heterochromatin-based silencing instead of a specific effect on the mutually exclusive *var* gene expression. As the silent *var* genes cluster into 6–8 foci with the telomeres in the nuclear periphery, their activation upon PfGCN5 BrD or PfPHD1 PHD deletion did not seem to involve their "moving" to a single transcriptionally competent locus, but rather appearing as multiple active *var* loci in the nuclear periphery. This is consistent with the observed expansion of the truncated PfGCN5 or

PfPHD1 to the outer nuclear compartments beyond the DAPI-stained central region. Moreover, the magnitude of all *var* transcripts compared with that in the WT parasite was significantly higher during PHD deletion (~25-fold) than during BrD deletion (~4-fold), which also agrees with the more severe effect of PHD deletion on the integrity of the PfGCN5 complex. This result emphasizes the fact that maintaining the spatial organization of the different chromatin domains in *P. falciparum* is crucial for regulating antigenic variation.

This study has demonstrated the power of the TAP procedure for more precisely identifying protein complexes in malaria parasites. The nine subunits identified in this study may constitute the major PfGCN5 complex in the late stages of the IDC, while multiple variants of the PfGCN5 complex may exist to carry out different biological functions. Single-step IP identified large numbers of additional, less abundant proteins, which may represent those that are either associated less tightly with the PfGCN5 core complex or are the subunits of variant PfGCN5 complexes. In particular, a conserved histone modification "reader" protein Pf14-3-3I (PF3D7_0818200) was also identified in the pulldowns with both PfGCN5 and PfPHD1. Pf14-3-3I binds to purified parasite histones and H3 phosphopeptides [108], and its potential binding to H3Ser10p may further favor the recruitment of the PfGCN5 complex to acetylate H3K14 as identified in yeast [109], pointing to the presence of extensive crosstalk of epigenetic marks in *P. falciparum*. Other identified proteins with the GCN5 complex are mostly associated with the biology of chromatins including components of the SWI-SNF chromatin-remodeling complex and proteins with histone-interacting domains (e.g., BrD, WD40, PHD, CHD). Their potential associations with the PfGCN5 complex highlight the complexity of epigenetic regulation of gene expression in *P. falciparum*.

This study revealed a unique GCN5 complex in a lower eukaryotic parasite that is drastically distinct from the SAGA complexes, which are evolutionarily conserved from yeast to human. The PfGCN5 complex, which is essential for regulating the stage-specific gene expression cascade, is also involved in the control of parasite-specific biological processes such as RBC invasion and virulence. The critical role of the PfGCN5 complex in parasite biology and its significant divergence from the human host suggests that the PfGCN5 complex may be a vital target for chemotherapy against malaria parasites. In this regard, efforts are directed at identifying selective molecules inhibiting the GCN5 enzyme activity and selective inhibitors disrupting the interaction between the PfGCN5 BrD and acetylated histones [110,111].

Material and methods

Parasite culture

The *P. falciparum* strain 3D7 and its genetically modified clones were cultured at 37˚C in a gas mixture of 5% CO_2, 3% O_2 and 92% N_2 with type O^+ RBCs at 5% hematocrit in RPMI 1640 medium supplemented with 25 mM $NaHCO_3$, 25 mM HEPES, 50 mg/L hypoxanthine, 0.5% Albumax II and 40 mg/ml gentamicin sulfate [112]. Synchronization of asexual stages was performed by two rounds of sorbitol treatment at the rings stage or by incubation of schizonts with RBCs for 3 h to obtain highly synchronized ring-stage parasites [113].

Genetic manipulation of *PfGCN5* and its associated genes

To tag the C-terminus of PfGCN5 with the PTP tag [65,66], the C-terminal *PfGCN5* fragment [nucleotides (nt) 3778–4758] was amplified from *P. falciparum* genomic DNA using primers F1 × R1. For the deletion of the PfGCN5 BrD and the PfPHD1 PHD domain, the *PfGCN5* fragment (nt 3286–4044) and the *PfPHD1* fragment (nt 3286–4044) were amplified using primers F2 × R2 and F3 × R3, respectively. All amplified fragments were first cloned into a modified pBluescript SK plasmid to fuse with the PTP or GFP and *pDT* 3' UTR as described earlier

[57,114]. This cassette was then subcloned into pHD22Y at *Bam*HI and *Not*I sites to produce pHD22Y/PfGCN-PTP, pHD22Y/GCN5-ΔBrD-GFP, and pHD22Y/PHD1-ΔPHD-GFP, respectively. A similar strategy was used to tag PfPHD1 with c-Myc and PF3D7_1019700 with GFP. All primers used for tagging, domain deletion, PCR verification of integration and probe for Southern blot are listed in **S9A Table**.

Parasite transfection was done using the RBC loading method [115]. Briefly, 100 μg of plasmid were introduced into fresh RBCs by electroporation. Purified schizonts were used to infect the RBCs pre-loaded with the plasmid and selection was done with 2.5 nM of WR99210 for approximately 4 weeks with weekly replenishment of fresh RBCs until resistant parasites appeared. Resistant parasites were subjected to three cycles of drug on-off selection and single clones of parasites with stable integration of the constructs were obtained by limiting dilution [113]. For the parasites transfected with constructs containing a GFP tag, fluorescence-activated cell sorting was employed to clone the GFP-positive parasites. Correct integrations of plasmids into the parasite genome were screened by integration-specific PCR or Southern blot with the digoxigenin (DIG)-labeled probes using an established protocol [80].

Purification of protein complexes

TAP was performed using the PTP-tagged PfGCN5 parasite line according to the published method [66]. Briefly, 10^9 parasites were lysed in 5 volumes of the hypotonic buffer (10 mM HEPES, pH 7.9, 1.5 mM $MgCl_2$, 10 mM KCl, 0.5 mM DTT, 0.5 mM EDTA) at 4˚C for 10 min followed by centrifugation for 20 min at $500 \times g$. The resultant pellet (nucleus) was further lysed in 5 volumes of PA150 buffer (150 mM KCl, 20 mM Tris-HCl, pH 7.7, 3 mM $MgCl_2$, 0.5 mM DTT, and 0.1% Tween 20) containing a protease inhibitor cocktail (Roche). The lysate was centrifuged for 10 min at $16,000 \times g$ and the supernatant was incubated with 100 μl (settled volume) of IgG agarose beads (GE Healthcare) at 4˚C for 2 h. The beads were washed twice with PA150 and equilibrated twice with the TEV buffer (150 mM KCl, 20 mM Tris-HCl, pH 7.7, 3 mM $MgCl_2$, 0.5 mM EDTA, 1 mM DTT, and 0.1% Tween 20). To release the PfGCN5 and its associated proteins from the IgG beads, the beads were incubated with 2 ml of TEV buffer containing 150 U of TEV protease and rotated overnight at 4˚C. The supernatant was collected, and the beads were rinsed with another 4 ml of the PC150 buffer (150 mM KCl, 20 mM Tris-HCl, pH 7.7, 3 mM MgCl2, 1 mM $CaCl_2$, 0.1% Tween 20). Then, 7.5 μl of 1 M $CaCl_2$ were added to titrate the EDTA from the TEV buffer and the combined supernatant was incubated with the anti-protein C beads for 2 h at 4˚C. The beads were washed four times with PC150 and eluted with the buffer containing 10 nM EGTA/5 mM EDTA. For the single-step pulldown of GFP-tagged or Myc-tagged protein, GFP- or Myc-trap (Cat# gta-20, RRID: AB_2631357 or Cat# yta-20, RRID:AB_2631369, Chromotek) beads were used with lysates from 10^9 parasites according to the manufacture's protocol.

Mass spectrometry

The proteins in the elution were concentrated by Amicon Ultra centrifugal filters (Millipore Sigma) and separated briefly in a 10% Bis-Tris SDS-PAGE gel for 10 min. Proteins in gel were excised, in-gel digested, and analyzed by nano-LC/MS/MS using a Waters NanoAcquity HPLC system interfaced to a Q Exactive Hybrid Quadrupole-Orbitrap Mass Spectrometer (Thermo Scientific) [116]. Peptides were loaded on a trapping column and eluted over a 75 μm analytical column at 350 nL/min. MS and MS/MS were performed at 70,000 FWHM and 17,500 FWHM resolutions, respectively. The fifteen most abundant ions were selected for MS/MS. Parasite proteins were identified by searching the Uniprot *P. falciparum* protein database (v01/2014). Data were filtered at 1% protein and 0.2% peptide FDR, and at least two

unique peptides per protein. Mascot DAT files were parsed into the Scaffold software for validation and filtering to create a non-redundant list per sample. The available mass spectrometry proteomics data have been deposited to the ProteomeXchange Consortium via the PRIDE [117] partner repository with the dataset identifier PXD023389 and 10.6019/PXD023389.

Antibody generation

To generate antibodies against PfPHD1 and PfPHD2, a PfPHD1 peptide (DNGKLQKVDGRKKRRYHK, aa 3685–3702) and a PfPHD2 peptide (DDNVKAEDYK-DENNDNDGD, aa 5738–5756) were synthesized and rabbits were immunized with these peptides. After three times immunizations, the antibodies were purified by affinity purification with peptides conjugated to the beads (Proteintech Group).

Gel filtration

To estimate the size of the PfGCN5 complex, nuclear extract from the PfGCN5::PTP was incubated with IgG beads, eluted by TEV protease cleavage as described above, and applied to a Superose 6 gel filtration column (GE Healthcare). Molecular mass standards (Gel Filtration Calibration Kit HMW, GE Healthcare) were run under the same conditions to estimate the size of the complex. The fractions were analyzed by Western blotting using antibodies against the PTP tag, PfPHD1 and PfPHD2, while HAT activity in the fractions was measured as described previously [57].

Growth phenotype analysis

The growth phenotypes of GCN5-ΔBrD::GFP and PHD1-ΔPHD::GFP lines during the IDC were compared with the WT 3D7 parasites as described [57]. To measure cell cycle progression, highly synchronous rings were obtained by incubation of purified schizonts with RBCs for 3 h. Progression of parasites through the IDC was monitored using Giemsa-stained smears every 2 h. Cycle time was determined as the duration between the peak ring parasitemias of two consecutive cycles. To measure parasite proliferation, synchronous cultures after two rounds of consecutive synchronization by sorbitol were initiated at 0.1% rings, and parasitemia was monitored daily for 7 days without replenishment of the RBCs. The number of merozoites produced per schizont was determined from mature segmenters. Three independent biological replications were done for each parasite line. Merozoite invasion assay was performed as described earlier [118]. Briefly, $\sim 1 \times 10^5$ of purified schizont from the WT, PfGCN5-ΔBrD:: GFP and PfPHD1-ΔPHD::GFP lines were mixed with $\sim 1 \times 10^7$ fresh RBCs, and the parasitemia of culture was determined 24 h later. The invasion rate was calculated as the percentage of merozoites invaded into RBCs assuming that each ruptured schizont releases an average of 10 merozoites using the formula: ring parasitemia × [(RBCs per μl)/(schizonts per μl ×10)]. To measure the gametocyte development, gametocyte induction was conducted by using an established method [80,119], and the gametocytemia was determined by counting gametocytes in Giemsa-stained thin blood smears at the middle developmental stage (stage III).

Histone modifications

To estimate histone modifications in the domain deletion mutants, histones were purified from the WT, GCN5-ΔBrD::GFP and PHD1-ΔPHD::GFP lines [120]. Equal amounts of the histones at each developmental stage were separated by 15% SDS/PAGE and transferred to nitrocellulose membranes. Western blotting was performed using a standard procedure with anti-acetyl histone H3, H3K9Ac (Catalog no. 07–352, RRID:AB_310544, Millipore), anti-tri

methyl histone H3, H3K4me3 (catalog no. 07–473, RRID:AB_1977252, Millipore) and anti-acetyl histone H4, H4Ac (catalog no. 06–598, RRID:AB_2295074, Millipore) at 1:1000 dilution as the primary antibodies and horseradish peroxidase-conjugated goat anti-rabbit IgG (diluted at 1:2000) as the secondary antibodies. The detected proteins were visualized using an enhanced chemiluminescence (ECL) kit (Invitrogen).

Immunofluorescence assay (IFA)

IFA was performed as described [121,122]. The parasitized RBCs were washed once with PBS and the cell pellet ($\sim$100 μl) was fixed with 1 ml of 4% (v/v) paraformaldehyde and 0.0075% (v/v) glutaraldehyde in PBS for 30 min followed by 10 min quenching with 50 mM glycine in PBS. Fixed cells were washed twice with PBS and treated with 0.5% (v/v) Triton X-100 in PBS for 10 min. Then, cells were washed twice with PBS and blocked in 3% (v/v) BSA for 1 h at room temperature. The anti-PfPHD1 (1 μg/ml), PfPHD2 antibodies (1 μg/ml), goat anti-GFP (1:2000; ab6673; Abcam, RRID:AB_305643, USA), mouse anti-Myc (ab56; Abcam, USA) and rabbit anti-H3K9ac (1:1000; 06–942, RRID:AB_310308, Millipore, USA) antibodies in PBS containing 1% BSA were added and incubated for another 1.5 h. After washing the cells three times with PBS, FITC-conjugated goat anti-rabbit IgG antibodies (Cat# F6005, RRID: AB_259682, Sigma, USA), Alexa fluor 488-conjugated secondary donkey anti-goat IgG antibody or Alexa fluor 594-conjugated secondary goat anti-rabbit antibody IgG antibody (A32814 RRID:AB_2762838 and R37117 RRID:AB_2556545, Thermo Fisher Scientific, USA) were added at 1:2000 dilution in 3% (v/v) BSA and incubated for 45 min. Nuclear staining was performed by incubating slides with 4',6-diamidino-2-phenylindole (DAPI, final 0.5 μg/mL; Invitrogen). Images were captured using an epifluorescence microscope (Nikon Eclipse Ni, USA; 100x/1.4 oil immersion lens) and were processed by Adobe Photoshop CS (Adobe Systems Inc. San José, CA). To quantitate co-localizations, images from at least 20 parasites were randomly selected, analyzed by ImageJ (1.52a; http://imagej.nih.gov/ij), and Pearson's coefficients were calculated.

Transcriptome analysis

To compare the transcriptomes during the IDC among the WT, GCN5-ΔBrD::GFP and PHD1-ΔPHD::GFP lines, RNA-seq was performed. Three replicates of total RNA from parasites at ring, early trophozoite, late trophozoite and schizont stages were harvested by using the ZYMO RNA purification kit, and used to generate the sequencing libraries using the KAPA Stranded mRNA Seq kit for the Illumina sequencing platform according to the manufacturer's protocol (KAPA biosystems). Libraries were sequenced on an Illumina HiSeq 2500 in the Rapid Run mode using 100 nt single read sequencing. Reads from Illumina sequencing were mapped to the *P. falciparum* genome sequence (Genedb v3.1) using HISAT2 [123]. Feature-Counts was utilized to calculate the read counts for each transcription in *P. falciparum* while the differential expression analysis was performed by DESeq2 [124,125] with the criteria of P-adjustment of <0.01 as the cutoff. RNA-seq data were also normalized by TPM to further validate the DEseq2 results. The differential expressed genes between domain deletion and WT are selected according to the following criteria: 1) the absolute fold change of TPM higher than 1 in all three biological replicates, and 2) P-adjustment from the DEseq lower than 0.01. The GO enrichment for up-regulated and down-regulated genes after BrD or PHD deletion was performed on PlasmDB (https://plasmodb.org/plasmo/). GSEA was performed as described [85,86] and the normalized enrichment score (NES) was used to measure the function enriched for a specific expression gene set. RNA-Seq data were submitted to NCBI GEO repository (accession number GSE164070).

Phaseogram of the transcriptomes of *P. falciparum* IDC

The sine wave model was utilized here to model the gene expression timing [126]. The gene transcription level from RNA-seq was first normalized as TPM (transcripts per million). Only the differential expressed genes in PfGCN5-ΔBrd or PfPHD1-ΔPHD as compared with WT were considered for the analysis. The TPM of each gene $E(t)$ was modeled as

$$E(t) = A \times \sin(\omega t - \alpha) + C \tag{1}$$

where $E(t) = [TPM_{12h}, TPM_{24h}, TPM_{36h}, TPM_{48h}]$ is the TPM at the $t = [12, 24, 36, 48]$ hours of sample collection, ω is the angular frequency and given by $\omega = 2\pi/48$, A is the amplitude of the expression profile, and C is the vertical offset of the profile from zero. To identify the parameter α and A, $A \times \sin(\omega t - \alpha)$ are changed to

$$A \times \sin(\omega t - \alpha) = \sin(\omega t) \times A \times \cos(-\alpha) + \cos(\omega t) \times A \times \sin(-\alpha) \tag{2}$$

Then the R command *lm* was used to fit a linear regression model between $E(t)$ and $\sin(\omega t) + \cos(\omega t)$. The fitting coefficient from the *lm* result indicates $A \times \cos(-\alpha)$ and $A \times \sin(-\alpha)$. The α and A were calculated as

$$\alpha = \text{arc} - \text{tangent} \left(\frac{A \times \sin(-\alpha)}{A \times \cos(-\alpha)} \right) \tag{3}$$

$$A = A \times \cos(-\alpha))^2 + (A \times \sin(-\alpha))^2 \tag{4}$$

The α indicates the horizontal offset of the profile from zero, which is used in the phaseogram to order the gene in the heatmap.

Association between chromatin structure and transcriptomic changes upon domain deletions

To quantify the association between open chromatin accessibility and transcriptional changes upon BrD deletion in PfGCN5 or PHD domain deletion in PfPHD1, we retrieved the ATAC-seq profile showing ATAC-seq peaks upstream the TSSs [52]. Each TSS was assigned to the nearest ATAC-seq peak with a distance restriction lower than 1 kb. The values of chromatin accessibility (ATAC-seq RPM + 0.1)/(gDNA RPM + 0.1) were then compared to the altered expression from the up- or down-regulated genes after domain deletions, where RPM represents the scaled reads per million reads. To investigate the association between the PfHP1 occupancy and transcriptional changes in the domain deletion mutants, the PfHP1 values (ChIP/input ratio) along the coding sequence were downloaded [95] and compared with the altered expression from the up and down-regulated gene after domain deletions.

ChIP quantitative PCR

ChIP-qPCR was performed as described [56,78,95] with some modifications. Synchronized GCN5-ΔBrD::GFP and PHD1-ΔPHD::GFP parasite lines at the ring stage [10–16 h post-invasion (hpi), ~5 × 10^9 infected RBCs (iRBCs)] and schizont stage (40–46 hpi, ~1.5 × 10^9 iRBCs) were harvested and crosslinked with paraformaldehyde (1% final concentration; EMS, USA) at 37°C for 15 min with agitation and then immediately neutralized by adding glycine (0.125 M final concentration) on ice for 5 min with agitation. The fixed iRBCs were lysed with saponin (0.06% final concentration; Sigma, USA) on ice for 5–10 min. Parasites were treated with a lysis buffer (10 mM KCl, 0.1 mM EDTA, 0.1 mM EGTA, 1 mM DTT, 10 mM Hepes pH 7.9, 1 × Protease inhibitor) and then gently homogenized using a douncer to free nuclei. Pelleted

nuclei were suspended in a shearing buffer (0.1% SDS, 5 mM EDTA, 50 mM Tris-HCl, pH 8.1, 1X Protease inhibitor) [95]. Sonication was performed using a rod bioruptor (Microson ultrasonic cell disruptor, Misonix, Inc. USA) at high power for 20 cycles of 30 sec ON/30 sec OFF, resulting in sheared chromatin of approximately 100–1000 bps. 50 μl of input samples was set aside before the remaining chromatin was diluted in incubation buffer (0.01% SDS, 1.5% Triton X-100, 0.5 mM EDTA, 200 mM NaCl, 5 mM Tris-HCl, pH 8.1). The chromatin (75 μl/400 ng) was incubated with goat anti-GFP (ab6673; Abcam), mouse anti-Myc (IgG2a monoclonal, ab56; Abcam), and their respective control antibodies (goat IgG, ab37373, mouse IgG2a, ab18413, Abcam) overnight at 4˚C while rotating followed by the addition of 20 μl of agarose beads for 1 h. Beads were then washed for 5 min at 4˚C while rotating with the following: buffer 1 (0.1% SDS, 1% Triton X-100, 150 mM NaCl, 2 mM EDTA, 20 mM Tris HCl, pH 8.1); buffer 2 (0.1% SDS, 1% Triton X-100, 500 mM NaCl, 2 mM EDTA, 20 mM Tris HCl, pH 8.1), buffer 3 (250 mM LiCl, 1% NP-40, 1% Na-deoxycholate, 1 mM EDTA, 10 mM Tris HCl, pH 8.1) and finally twice with buffer 4 (10 mM EDTA, 10 mM Tris HCl, pH 8). The immunoprecipitated (IPed) chromatin was eluted with the elution buffer (1% SDS, 0.1M NaHCO$_3$) at room temperature for 15 min with rotation. The eluted chromatin and input samples were reverse cross-linked in 10% SDS, 1 M NaHCO$_3$, 5 M NaCl, 10% Triton X-100 at 45˚C overnight while shaking and purified by the phenol:chloroform method. For qPCR, the concentration of immunoprecipitated gDNA was determined by Qubit dsDNA Broad-Range Assay Kit (Invitrogen, USA), and 10 ng per well in triplicate were used for qPCR using the FastStart Universal SYBR Green Master [Rox] (Sigma-Aldrich, USA) as described [56]. Primer pairs targeting 5′UTRs were designed to amplify fragments less than 200 bp (**S9B Table**). Fold enrichment relative to constitutively expressed reference gene *seryl-tRNA synthetase* (*stRNA*, PF3D7_0717700) was calculated by using the $2^{-\Delta\Delta Ct}$ method [127]. The fold changes of binding enrichment were calculated using a formula: $2^{-[(\text{IP Ct-}target - \text{IP Ct-}stRNA)-(\text{control IP Ct-}target-\text{control IP Ct-}stRNA)]}$ for each primer set targeting specific promoter regions.

RNA fluorescent in-situ hybridization (FISH)

RNA FISH was performed as described [35]. Briefly, purified ring-stage parasites were lysed with saponin and released parasites fixed in suspension with ice-cold 4% paraformaldehyde. Parasites were then deposited on Teflon-coated microscope slides and hybridized with denatured *var* probes at 42˚C for at least 16 h. All the FISH probes were PCR amplified from genomic DNA using the primers listed in S9B Table. The slides were then washed three times in 2×SSC at 42˚C. Finally, the slides were incubated with streptavidin-488 antibody at room temperature for 30 min. Images were taken using a Nikon ECLIPSE E600 epifluorescence microscope. NIS Elements 3.0 software was used for acquisition and ImageJ for composition.

Statistical analysis

For all experiments, three or more independent biological replicates were performed. The results are presented as mean ± SD. Results are regarded significant if $P < 0.05$ as established by ANOVA, Fisher's exact test, paired Mann Whitney U test or paired Wilcoxon test, and the respective analysis was shown in the figure legends. To analyze the schizont numbers containing different numbers of merozoites, a χ^2 goodness of fit test was first used to evaluate if the number of schizonts that contain a certain number of merozoites was independent of the parasite lines. Then the proportions of schizonts with a certain number of merozoites were compared among these cell lines based on ANOVA for each merozoite number.

Supporting information

S1 Fig. PfGCN5::PTP tagging, PfGCN5 expression and localization during development, and tandem affinity purification (TAP) of the PfGCN5 complex. (A) Schematic diagram of PTP tagging at C-terminal of PfGCN5. P1 and P2 are primers used for verification of integration by PCR. **(B)** Cartoon shows the TAP procedure for purification of the PfGCN5 complex. A, B, and C are subunits of the GCN5 complex. TEV: tobacco etch virus protease. **(C)** Integration-specific PCR verification of two positive clones (C1 and C3) from transfected parasites. **(D)** Western blot detecting PfGCN5::PTP expression in the recombinant parasite clone C3 at different developmental stages (R: ring; ET: early trophozoite; LT: late trophozoite; S: schizont). The blot was probed with antibodies against protein C. Molecular markers in kDa are shown on the left. The expression of aldolase was used as a loading control. The PfGCN5::PTP protein bands are indicated by asterisks. **(E)** Live cell imaging shows the localization of PfGCN5::GFP during intraerythrocytic development (R: ring; ET: early trophozoite; LT: late trophozoite; ES: early schizont; LS: late schizont). DAPI was used to stain nucleus. BF, bright field. Scale bar = 5 μm.
(PDF)

S2 Fig. PHD domains in PfPHD1 and PfPHD2 proteins. (A) Sequence of four PHD domains in PfPHD1, C and H amino acid residues in the PHD domain are highlighted underneath the sequence. PHD-SF: PHD superfamily; ePHD: elongated PHD domain, PHD_TAF3: TAF3 type PHD domain. **(B)** Sequences of four PHD domains in PfPHD2. **(C)** Alignment of PfPHD1 PHD_TAF3 domain with other known authentic PHD domains which bind H3K4me3/2. The alignment shows the conserved Zinc-binding residues in light gray for Zinc 1 and dark gray for Zinc 2, and the two core β-strands in green. The residues involved in H3K4me3 recognition are labeled I through V (forming the aromatic cages) and the aromatic residues in the recognition cage are shadowed in green. MLL1: mixed-lineage leukemia-1; JARID1A: jumonji, AT-rich interactive domain 1A; PYGO: pygopus homolog 1; BPTF: bromodomain PHD finger transcription factor; PHF2: PHD finger protein 2; Yng1: yeast homolog of mammalian ING1; ING4: inhibitor of growth protein 4; TAF3: transcription initiation factor TFIID subunit 3.
(PDF)

S3 Fig. Association of PfPHD1 or PfPHD2 with PfGCN5. (A) The nuclear localization of PfPHD1 and PfPHD2 were interrogated by IFA using anti-PfPHD1 and PfPHD2 antibodies. Nuclei were counter-stained by DAPI. Scale bar = 5 μm. BF, bright field. **(B)** Immunoprecipitation (IP) of proteins from lysates of the PfGCN5::PTP parasite line using agarose conjugated with either anti-PfPHD1 or PfPHD2 antibodies. IPed proteins were separated by SDS-PAGE and probed with anti-Protein C antibodies recognizing the full-length GCN5::PTP. Preimmune sera were used as controls. **(C)** IP of proteins from lysates of the 3D7 wild-type parasites using agarose conjugated with anti-PfPHD1 (left panel) or PfPHD2 (right panel) antibodies. IPed proteins were separated by SDS-PAGE and probed with anti-PfPHD2 or anti-PfPHD1 antibodies.
(PDF)

S4 Fig. Tagging of PfPHD1 (PF3D7_1008100) with c-Myc. (A) Schematic diagram of Myc tagging at C-terminal of PfPHD1. A, AvrII; S, StuI. **(B)** Southern blot of 3D7 and three transgenic clones (1–3). Genomic DNA was digested with AvrII and StuI and hybridized with labeled DNA shown as "Probe" in **A**. **(C)** Western blot analysis of nuclear (Nu) and cytoplasmic (Cyto) protein extracts with antibodies against the Myc tag, aldolase (for cytoplasmic

compartment) and histone H3 (for nuclear compartment).
(PDF)

S5 Fig. Tagging of PF3D7_1019700) with GFP and pulldown of associated proteins. (A)
The diagram shows GFP tagging of the PF3D7_1019700 at its C-terminus by single-crossover homologous recombination. Purple blocks show the fragment used for homologous recombination. (**B**) Integration-specific PCR using primers P1 and P2. WT, Wildtype 3D7; C1 and C2 are two transgenic clones**. (C)** Live cell imaging shows the localization of PF3D7_1019700:: GFP in the nuclei by fluorescence microscopy. R: ring; ET: early trophozoite; LT: late trophozoite; ES: early schizont; LS: late schizont. (**D**) Proteins identified from parasite nuclear extracts by IP and LC-MS/MS. Single-step IPs with anti-GFP beads were done using the PF3D7_1019700::GFP (R1 and R2 indicate two replicates). The wild-type 3D7 was used as the IP control. The proteomic data were analyzed by SAINT using a threshold of probability >94% and 1% FDR. Gene ID and annotations are shown on the right.
(PDF)

S6 Fig. Deletion of PfGCN5 Bromodomain (BrD) and the PfPHD1 PHD-TAF3 domain.
(**A**) Schematic showing BrD deletion by single crossover homologous recombination. (**B**) Southern blot analysis of three positive clones from transfected parasites. Genomic DNA was digested with AvrII and SpeI, and hybridized to the probe marked in **A**. (**C**) Schematic showing the deletion of PHD-TAF3 domain. (**D**) Southern blot of two positive clones from transfected parasites. Genomic DNA was digested with SpeI and XhoI, and hybridized to the probe marked in C. In both cases, GFP was tagged at the ends of truncated genes. (**E**) Western blot shows the size changes of the truncated GCN5 protein bands and the reduced expression levels after BrD deletion. (**F**)**.** Images of Giemsa-stained films of parasite cultures synchronized at the ring stage to show the extended IDC of the two domain deletion parasite lines. (**G**) Live cell imaging shows GFP signals in parasites with truncated GCN5 in the GCN5-ΔBrd::GFP parasite line. Compared to S1E Fig, the GCN5-ΔBrd-GFP protein shows weaker fluorescence and a more diffused nuclear localization pattern. Scale bar = 5 μm. (**H**) Localization of truncated PfPHD1 in PHD1-ΔPHD::GFP parasite line. Scale bar = 5 μm. R, ET, LT and S denote ring, early trophozoite, late trophozoite and schizont stages, respectively. BF, bright field.
(PDF)

S7 Fig. PfPHD1 and H3K9ac localization in parasites before and after PHD deletion in PfPHD1. (A) IFA images show high-degree co-localization of PfPHD1, H3K9ac and euchromatin (DAPI) in the nucleus in parasite line with c-Myc-tagged PfPHD1. Numbers indicate the levels of signal correlation between two markers. Scale bar = 5 μm. (**B**) IFA shows decreased co-localization of PfPHD1, H3K9ac and euchromatin (denoted by DAPI staining) after PHD1 PHD domain deletion. Scale bar = 5 μm. R, ring; T, trophozoite; S, schizont. (**C**) The intensities of H3K9ac in the 1N or 2N+ single nucleus of wild-type (WT), PfGCN5-ΔBrD::GFP, and PfPHD1-ΔPHD::GFP trophozoite. The copy number (1N or 2N+) in a single nucleus of trophozoite was defined by the intensity of DAPI signal compared to the 1N nucleus of the ring. Bars indicate means and standard deviations (n = 12). The statistical difference was evaluated by Mann–Whitney U test.
(PDF)

S8 Fig. The effect of domain deletions in PfGCN5 and PfPHD1 on transcription. (A–D)
Volcano plots show the genes with altered transcription at the early trophozoite (**A**) and late trophozoite (**B**) stages in PfGCN5-ΔBrD, and at the early trophozoite (**C**) and late trophozoite (**D**) stages in PfPHD1-ΔPHD. (**E**) Pearson correlation in fold change between PfGCN5-ΔBrD

and PfPHD1-ΔPHD in different developmental stages.
(PDF)

S9 Fig. Transcriptional alteration upon domain deletions. Gene ontology enrichment analysis of up- (**A, C**) and down-regulated (**B, D**) genes in PfGCN5-ΔBrD (A, B) and PfPHD1-ΔPHD (C, D) parasites compared to the wildtype 3D7.
(PDF)

S10 Fig. Transcriptional alteration in different categories of genes upon domain deletions. (**A-D**) Heatmaps display the alteration of gene transcription showing normalized z-scores to illustrate the gene expression cascade observed in 3D7 and those in mutant parasite lines. (**A**) Genes associated with protein translation and gene transcription. (**B**) Genes involved in the invasion of RBCs. (**C**) AP2-family genes. (**D**) Genes specifically expression in gametocytes and ookinetes. (**E**) The number of up- and down-regulated genes upon PfPHD1 PHD domain deletion are shown as the red and blue bars at four developmental stages. These altered genes were further classified as the putative target genes of AP2-LT and the remaining genes. The putative target genes of AP2-LT were significantly enriched in those down-regulated genes in the late stages of PfPHD1-ΔPHD::GFP parasites. R, ring; ET, early trophozoite; LT, late trophozoite; S, schizont. ***, $P < 0.001$ (Fisher's exact test).
(PDF)

S11 Fig. Enrichment of PfGCN5 or PfPHD1 at the promoters of genes was correlated with the activation status of the genes. Genes selected for evaluation include *MSP1* (**A**), *VAR2CSA* (**B**), and the sexual-stage gene *Pfg27/25* (**C**). The enrichment was determined by chromatin-immunoprecipitation (ChIP) followed by qPCR using primer pairs marked as 1, 2, 3, or 4 located in the promoters of the respective genes. The fold change indicates the enrichment relative to constitutively expressed reference gene *seryl-tRNA synthetase* (PF3D7_0717700). (**A**) Upon domain deletion, PfGCN5-ΔBrD and PfPHD1-ΔPHD were depleted in the promoters of *MSP1* at the schizont (central panels) but enriched at the ring stage (left panels). The right panels show the ratio of enrichments between domain deletions (PfGCN5-ΔBrD::GFP and PfPHD1-ΔPHD::GFP) and their wild-type parasites (PfGCN5::GFP and PfPHD1::myc). (**B, C**) At the ring stage, PfGCN5-ΔBrD and PfPHD1-ΔPHD were enriched at the promoters of *var2csa* (**B**) and *Pfg27/25* (**C**). (*, **, and *** indicate $P < 0.05$, 0.01 and 0.001, respectively, Mann-Whitney U test).
(PDF)

S12 Fig. Enrichment of H3K9ac and depletion of H3K9me3 at the promoters of HP1-controlled, heterochromatic genes. Selected HP1-controlled genes for evaluation include *var2csa* (**A**) and *rifin* (*PF3D7_1000200*) (**B**). Enrichment was determined at the ring stage by ChIP followed by qPCR using primer pairs marked as 1, 2, and 3 located in the promoters of the respective genes. The fold change indicates the enrichment relative to constitutively expressed reference gene *seryl-tRNA synthetase* (PF3D7_0717700). (**A**) H3K9me3 was depleted in the promoters of *var2csa* upon PfGCN5 BrD and PfPHD1 PHD deletion (upper panel) compared to the wild-type parasites (PfGCN5::GFP and PfPHD1::myc), whereas H3K9ac was enriched in both deletion mutants (lower panel). (**B**) Depletion of H3K9me3 and enrichment of H3K9ac were observed at certain positions of the *rifin* promoter upon BrD and PHD deletion, respectively.
(PDF)

S1 Table. Proteomic analyses of GCN5 associated complex. (**A**) Proteomic data from GCN5-PTP TAPs. (**B**) SAINT analysis of GCN5-PTP TAPs. (**C**) Proteomic data from

PHD1-Myc IPs. (**D**) SAINT analysis of PHD1-Myc IPs. (**E**) Proteomic data from PF3D7_1019700-GFP IPs. (**F**) SAINT analysis of PF3D7_1019700-GFP IPs. (**G**) Proteomic data from PfGCN5-GFP IPs at ring stage. (**H**) SAINT analysis of PfGCN5-GFP IPs. (XLSX)

S2 Table. Proteomic analyses of GCN5 associated complex after domain deletions. (**A**) Proteomic data from GCN5-GFP IPs. (**B**) SAINT analysis of GCN5-GFP IPs. (**C**) Proteomic data from GCN5-ΔBrD-GFP IPs. (**D**) SAINT analysis of GCN5-ΔBrD-GFP IPs IPs. (**E**) Proteomic data from PHD1-ΔPHD-GFP IPs. (**F**) SAINT analysis of PHD1-ΔPHD-GFP IPs. (XLSX)

S3 Table. Transcriptome data of GCN5-ΔBrD::GFP line as compared to 3D7 wildtype. Deseq2 and TPM analysis of three replicates of RNAseq data at ring (**A**), early trophozoite (**B**), late trophozoite (**C**) and schizont (**D**) stages. (XLSX)

S4 Table. Transcriptome data of PHD1-ΔPHD::GFP line as compared to 3D7 wildtype. Deseq2 and TPM analysis of three replicates of RNAseq data at ring (**A**), early trophozoite (**B**), late trophozoite (**C**) and schizont (**D**) stages. (XLSX)

S5 Table. GO enrichment analyses of altered genes upon domain deletions. (**A**) GO enrichment analyses of altered genes upon BrD domain deletion in GCN5. (**B**) GO enrichment analyses of altered genes upon PHD domain deletion in PHD1. (**C**) GSEA of altered genes upon BrD domain deletion in GCN5. (**D**) Summary of GSEA on GCN5-ΔBrD. (**E**) GSEA of altered genes upon PHD domain deletion in PHD1. (**F**) Summary of GSEA on PHD1-ΔPHD. (XLSX)

S6 Table. Transcriptional alteration of different biological pathways upon domain deletions. (**A**) Up-regulation of *var* gene expression at early asexual stage upon domain deletions. (**B**) Down-regulation of invasion-related genes upon domain deletions. (**C**) Down-regulation of translation-related genes upon domain deletions. (**D**) Downregulation of transcription-related genes upon domain deletions. (**E**) Alteration of AP2 gene expression upon domain deletions. (XLSX)

S7 Table. Transcriptional escalation of HP1 controlled genes upon domain deletions. (XLSX)

S8 Table. Transcriptional escalation of gametocyte and ookinete specific genes upon domain deletions. (XLSX)

S9 Table. Primers list. (**A**) for tagging, domain deletion, integration checking, and probe. (**B**) for ChIP-qPCR and FISH. (XLSX)

Acknowledgments

Author Contributions

Conceptualization: Jun Miao, Kami Kim, Liwang Cui.

Data curation: Jun Miao, Chengqi Wang, Amuza Byaruhanga Lucky, Xiaoying Liang, Swamy Rakesh Adapa.

Formal analysis: Jun Miao, Chengqi Wang, Amuza Byaruhanga Lucky, Swamy Rakesh Adapa, Rays Jiang.

Funding acquisition: Jun Miao, Liwang Cui.

Investigation: Jun Miao, Amuza Byaruhanga Lucky, Xiaoying Liang, Hui Min.

Methodology: Jun Miao, Amuza Byaruhanga Lucky, Xiaoying Liang, Hui Min.

Supervision: Jun Miao, Rays Jiang, Kami Kim, Liwang Cui.

Validation: Amuza Byaruhanga Lucky, Hui Min.

Writing – original draft: Jun Miao, Liwang Cui.

Writing – review & editing: Jun Miao, Rays Jiang, Kami Kim, Liwang Cui.

References

1. Bannister AJ, Kouzarides T. Regulation of chromatin by histone modifications. Cell Res. 2011; 21 (3):381–95. Epub 2011/02/16. https://doi.org/10.1038/cr.2011.22 PMID: 21321607; PubMed Central PMCID: PMC3193420.

2. Strahl BD, Allis CD. The language of covalent histone modifications. Nature. 2000; 403(6765):41–5. Epub 2000/01/19. https://doi.org/10.1038/47412 PMID: 10638745.

3. Jenuwein T, Allis CD. Translating the histone code. Science. 2001; 293(5532):1074–80. Epub 2001/08/11. https://doi.org/10.1126/science.1063127 PMID: 11498575.

4. Winter S, Fischle W. Epigenetic markers and their cross-talk. Essays Biochem. 2010; 48(1):45–61. Epub 2010/09/09. https://doi.org/10.1042/bse0480045 PMID: 20822485.

5. Lee JS, Smith E, Shilatifard A. The language of histone crosstalk. Cell. 2010; 142(5):682–5. Epub 2010/09/04. https://doi.org/10.1016/j.cell.2010.08.011 PMID: 20813257; PubMed Central PMCID: PMC3711869.

6. Murr R. Interplay between different epigenetic modifications and mechanisms. Adv Genet. 2010; 70:101–41. Epub 2010/10/06. https://doi.org/10.1016/B978-0-12-380866-0.60005-8 PMID: 20920747.

7. Marmorstein R, Zhou MM. Writers and readers of histone acetylation: structure, mechanism, and inhibition. Cold Spring Harbor perspectives in biology. 2014; 6(7):a018762. Epub 2014/07/06. https://doi.org/10.1101/cshperspect.a018762 PMID: 24984779; PubMed Central PMCID: PMC4067988.

8. Grant PA, Duggan L, Cote J, Roberts SM, Brownell JE, Candau R, et al. Yeast Gcn5 functions in two multisubunit complexes to acetylate nucleosomal histones: characterization of an Ada complex and the SAGA (Spt/Ada) complex. Genes & development. 1997; 11(13):1640–50. Epub 1997/07/01. https://doi.org/10.1101/gad.11.13.1640 PMID: 9224714.

9. Helmlinger D, Tora L. Sharing the SAGA. Trends Biochem Sci. 2017; 42(11):850–61. Epub 2017/10/02. https://doi.org/10.1016/j.tibs.2017.09.001 PMID: 28964624; PubMed Central PMCID: PMC5660625.

10. Spedale G, Timmers HT, Pijnappel WW. ATAC-king the complexity of SAGA during evolution. Genes Dev. 2012; 26(6):527–41. Epub 2012/03/20. https://doi.org/10.1101/gad.184705.111 PMID: 22426530; PubMed Central PMCID: PMC3315114.

11. Wang J, Dixon SE, Ting LM, Liu TK, Jeffers V, Croken MM, et al. Lysine acetyltransferase GCN5b interacts with AP2 factors and is required for Toxoplasma gondii proliferation. PLoS Pathog. 2014; 10 (1):e1003830. Epub 2014/01/07. https://doi.org/10.1371/journal.ppat.1003830 PMID: 24391497; PubMed Central PMCID: PMC3879359.

12. Harris MT, Jeffers V, Martynowicz J, True JD, Mosley AL, Sullivan WJ Jr., A novel GCN5b lysine acetyltransferase complex associates with distinct transcription factors in the protozoan parasite Toxoplasma gondii. Mol Biochem Parasitol. 2019; 232:111203. Epub 2019/08/06. https://doi.org/10.1016/j.molbiopara.2019.111203 PMID: 31381949; PubMed Central PMCID: PMC6717552.

13. Mao Y, Pavangadkar KA, Thomashow MF, Triezenberg SJ. Physical and functional interactions of Arabidopsis ADA2 transcriptional coactivator proteins with the acetyltransferase GCN5 and with the cold-induced transcription factor CBF1. Biochim Biophys Acta. 2006; 1759(1–2):69–79. Epub 2006/04/11. https://doi.org/10.1016/j.bbaexp.2006.02.006 PMID: 16603259.

14. Moraga F, Aquea F. Composition of the SAGA complex in plants and its role in controlling gene expression in response to abiotic stresses. Front Plant Sci. 2015; 6:865. Epub 2015/11/04. https://doi.org/10.3389/fpls.2015.00865 PMID: 26528322; PubMed Central PMCID: PMC4604261.

15. Huisinga KL, Pugh BF. A genome-wide housekeeping role for TFIID and a highly regulated stress-related role for SAGA in Saccharomyces cerevisiae. Mol Cell. 2004; 13(4):573–85. Epub 2004/03/03. https://doi.org/10.1016/s1097-2765(04)00087-5 PMID: 14992726.

16. Vlachonasios KE, Thomashow MF, Triezenberg SJ. Disruption mutations of ADA2b and GCN5 transcriptional adaptor genes dramatically affect Arabidopsis growth, development, and gene expression. Plant Cell. 2003; 15(3):626–38. Epub 2003/03/05. https://doi.org/10.1105/tpc.007922 PMID: 12615937; PubMed Central PMCID: PMC150018.

17. Bonnet J, Wang CY, Baptista T, Vincent SD, Hsiao WC, Stierle M, et al. The SAGA coactivator complex acts on the whole transcribed genome and is required for RNA polymerase II transcription. Genes Dev. 2014; 28(18):1999–2012. Epub 2014/09/18. https://doi.org/10.1101/gad.250225.114 PMID: 25228644; PubMed Central PMCID: PMC4173158.

18. Baptista T, Grunberg S, Minoungou N, Koster MJE, Timmers HTM, Hahn S, et al. SAGA Is a General Cofactor for RNA Polymerase II Transcription. Mol Cell. 2017; 68(1):130–43 e5. Epub 2017/09/19. https://doi.org/10.1016/j.molcel.2017.08.016 PMID: 28918903; PubMed Central PMCID: PMC5632562.

19. Koutelou E, Hirsch CL, Dent SY. Multiple faces of the SAGA complex. Curr Opin Cell Biol. 2010; 22 (3):374–82. Epub 2010/04/07. https://doi.org/10.1016/j.ceb.2010.03.005 PMID: 20363118; PubMed Central PMCID: PMC2900470.

20. WHO. Would Malaria Report 2020. Geneva: WHO. 2020.

21. Hall N, Karras M, Raine JD, Carlton JM, Kooij TW, Berriman M, et al. A comprehensive survey of the Plasmodium life cycle by genomic, transcriptomic, and proteomic analyses. Science. 2005; 307 (5706):82–6. Epub 2005/01/08. https://doi.org/10.1126/science.1103717 PMID: 15637271.

22. Bozdech Z, Llinas M, Pulliam BL, Wong ED, Zhu J, DeRisi JL. The transcriptome of the intraerythrocytic developmental cycle of Plasmodium falciparum. PLoS Biol. 2003; 1(1):E5. Epub 2003/08/21. https://doi.org/10.1371/journal.pbio.0000005 PMID: 12929205; PubMed Central PMCID: PMC176545.

23. Le Roch KG, Zhou Y, Blair PL, Grainger M, Moch JK, Haynes JD, et al. Discovery of gene function by expression profiling of the malaria parasite life cycle. Science. 2003; 301(5639):1503–8. Epub 2003/08/02. https://doi.org/10.1126/science.1087025 PMID: 12893887.

24. Cortes A, Deitsch KW. Malaria Epigenetics. Cold Spring Harb Perspect Med. 2017; 7(7). Epub 2017/03/23. https://doi.org/10.1101/cshperspect.a025528 PMID: 28320828; PubMed Central PMCID: PMC5495052.

25. Gupta AP, Bozdech Z. Epigenetic landscapes underlining global patterns of gene expression in the human malaria parasite, Plasmodium falciparum. Int J Parasitol. 2017; 47(7):399–407. Epub 2017/04/18. https://doi.org/10.1016/j.ijpara.2016.10.008 PMID: 28414071.

26. Batugedara G, Lu XM, Bunnik EM, Le Roch KG. The Role of Chromatin Structure in Gene Regulation of the Human Malaria Parasite. Trends Parasitol. 2017; 33(5):364–77. Epub 2017/01/10. https://doi.org/10.1016/j.pt.2016.12.004 PMID: 28065669; PubMed Central PMCID: PMC5410391.

27. Voss TS, Bozdech Z, Bartfai R. Epigenetic memory takes center stage in the survival strategy of malaria parasites. Curr Opin Microbiol. 2014; 20:88–95. Epub 2014/06/20. https://doi.org/10.1016/j.mib.2014.05.007 PMID: 24945736.

28. Vembar SS, Scherf A, Siegel TN. Noncoding RNAs as emerging regulators of Plasmodium falciparum virulence gene expression. Curr Opin Microbiol. 2014; 20:153–61. Epub 2014/07/16. https://doi.org/10.1016/j.mib.2014.06.013 PMID: 25022240; PubMed Central PMCID: PMC4157322.

29. Callebaut I, Prat K, Meurice E, Mornon JP, Tomavo S. Prediction of the general transcription factors associated with RNA polymerase II in Plasmodium falciparum: conserved features and differences relative to other eukaryotes. BMC Genomics. 2005; 6:100. Epub 2005/07/27. https://doi.org/10.1186/1471-2164-6-100 PMID: 16042788; PubMed Central PMCID: PMC1199594.

30. Coulson RM, Hall N, Ouzounis CA. Comparative genomics of transcriptional control in the human malaria parasite Plasmodium falciparum. Genome Res. 2004; 14(8):1548–54. Epub 2004/07/17. https://doi.org/10.1101/gr.2218604 PMID: 15256513; PubMed Central PMCID: PMC509263.

31. de Boer CG, Hughes TR. YeTFaSCo: a database of evaluated yeast transcription factor sequence specificities. Nucleic acids research. 2012; 40(Database issue):D169–79. Epub 2011/11/22. https://doi.org/10.1093/nar/gkr993 PMID: 22102575; PubMed Central PMCID: PMC3245003.

32. Balaji S, Babu MM, Iyer LM, Aravind L. Discovery of the principal specific transcription factors of Apicomplexa and their implication for the evolution of the AP2-integrase DNA binding domains. Nucleic Acids Res. 2005; 33(13):3994–4006. Epub 2005/07/26. https://doi.org/10.1093/nar/gki709 PMID: 16040597; PubMed Central PMCID: PMC1178005.

33. Campbell TL, De Silva EK, Olszewski KL, Elemento O, Llinas M. Identification and genome-wide prediction of DNA binding specificities for the ApiAP2 family of regulators from the malaria parasite. PLoS Pathog. 2010; 6(10):e1001165. Epub 2010/11/10. https://doi.org/10.1371/journal.ppat.1001165 PMID: 21060817; PubMed Central PMCID: PMC2965767.

34. Cui L, Miao J. Chromatin-mediated epigenetic regulation in the malaria parasite Plasmodium falciparum. Eukaryot Cell. 2010; 9(8):1138–49. Epub 2010/05/11. https://doi.org/10.1128/EC.00036-10 PMID: 20453074; PubMed Central PMCID: PMC2918932.

35. Lopez-Rubio JJ, Mancio-Silva L, Scherf A. Genome-wide analysis of heterochromatin associates clonally variant gene regulation with perinuclear repressive centers in malaria parasites. Cell Host Microbe. 2009; 5(2):179–90. Epub 2009/02/17. https://doi.org/10.1016/j.chom.2008.12.012 PMID: 19218088.

36. Salcedo-Amaya AM, van Driel MA, Alako BT, Trelle MB, van den Elzen AM, Cohen AM, et al. Dynamic histone H3 epigenome marking during the intraerythrocytic cycle of Plasmodium falciparum. Proc Natl Acad Sci U S A. 2009; 106(24):9655–60. Epub 2009/06/06. https://doi.org/10.1073/pnas.0902515106 PMID: 19497874; PubMed Central PMCID: PMC2701018.

37. Ay F, Bunnik EM, Varoquaux N, Bol SM, Prudhomme J, Vert JP, et al. Three-dimensional modeling of the P. falciparum genome during the erythrocytic cycle reveals a strong connection between genome architecture and gene expression. Genome Res. 2014; 24(6):974–88. Epub 2014/03/29. https://doi.org/10.1101/gr.169417.113 PMID: 24671853; PubMed Central PMCID: PMC4032861.

38. Freitas-Junior LH, Bottius E, Pirrit LA, Deitsch KW, Scheidig C, Guinet F, et al. Frequent ectopic recombination of virulence factor genes in telomeric chromosome clusters of P. falciparum. Nature. 2000; 407(6807):1018–22. Epub 2000/11/09. https://doi.org/10.1038/35039531 PMID: 11069183.

39. Bunnik EM, Venkat A, Shao J, McGovern KE, Batugedara G, Worth D, et al. Comparative 3D genome organization in apicomplexan parasites. Proc Natl Acad Sci U S A. 2019; 116(8):3183–92. Epub 2019/02/07. https://doi.org/10.1073/pnas.1810815116 PMID: 30723152; PubMed Central PMCID: PMC6386730.

40. Bunnik EM, Cook KB, Varoquaux N, Batugedara G, Prudhomme J, Cort A, et al. Changes in genome organization of parasite-specific gene families during the Plasmodium transmission stages. Nat Commun. 2018; 9(1):1910. Epub 2018/05/17. https://doi.org/10.1038/s41467-018-04295-5 PMID: 29765020; PubMed Central PMCID: PMC5954139.

41. Crowley VM, Rovira-Graells N, Ribas de Pouplana L, Cortes A. Heterochromatin formation in bistable chromatin domains controls the epigenetic repression of clonally variant Plasmodium falciparum genes linked to erythrocyte invasion. Mol Microbiol. 2011; 80(2):391–406. Epub 2011/02/11. https://doi.org/10.1111/j.1365-2958.2011.07574.x PMID: 21306446.

42. Freitas-Junior LH, Hernandez-Rivas R, Ralph SA, Montiel-Condado D, Ruvalcaba-Salazar OK, Rojas-Meza AP, et al. Telomeric heterochromatin propagation and histone acetylation control mutually exclusive expression of antigenic variation genes in malaria parasites. Cell. 2005; 121(1):25–36. Epub 2005/04/12. https://doi.org/10.1016/j.cell.2005.01.037 PMID: 15820676.

43. Chookajorn T, Dzikowski R, Frank M, Li F, Jiwani AZ, Hartl DL, et al. Epigenetic memory at malaria virulence genes. Proc Natl Acad Sci U S A. 2007; 104(3):899–902. Epub 2007/01/09. https://doi.org/10.1073/pnas.0609084103 PMID: 17209011; PubMed Central PMCID: PMC1764221.

44. Perez-Toledo K, Rojas-Meza AP, Mancio-Silva L, Hernandez-Cuevas NA, Delgadillo DM, Vargas M, et al. Plasmodium falciparum heterochromatin protein 1 binds to tri-methylated histone 3 lysine 9 and is linked to mutually exclusive expression of var genes. Nucleic Acids Res. 2009; 37(8):2596–606. Epub 2009/03/10. https://doi.org/10.1093/nar/gkp115 PMID: 19270070; PubMed Central PMCID: PMC2677873.

45. Flueck C, Bartfai R, Volz J, Niederwieser I, Salcedo-Amaya AM, Alako BT, et al. Plasmodium falciparum heterochromatin protein 1 marks genomic loci linked to phenotypic variation of exported virulence factors. PLoS Pathog. 2009; 5(9):e1000569. Epub 2009/09/05. https://doi.org/10.1371/journal.ppat.1000569 PMID: 19730695; PubMed Central PMCID: PMC2731224.

46. Brancucci NMB, Bertschi NL, Zhu L, Niederwieser I, Chin WH, Wampfler R, et al. Heterochromatin protein 1 secures survival and transmission of malaria parasites. Cell Host Microbe. 2014; 16(2):165–76. Epub 2014/08/15. https://doi.org/10.1016/j.chom.2014.07.004 PMID: 25121746.

47. Ponts N, Harris EY, Lonardi S, Le Roch KG. Nucleosome occupancy at transcription start sites in the human malaria parasite: a hard-wired evolution of virulence? Infect Genet Evol. 2011; 11(4):716–24. Epub 2010/08/17. https://doi.org/10.1016/j.meegid.2010.08.002 PMID: 20708104; PubMed Central PMCID: PMC3466077.

48. Bunnik EM, Polishko A, Prudhomme J, Ponts N, Gill SS, Lonardi S, et al. DNA-encoded nucleosome occupancy is associated with transcription levels in the human malaria parasite Plasmodium falciparum. BMC Genomics. 2014; 15:347. Epub 2014/06/03. https://doi.org/10.1186/1471-2164-15-347 PMID: 24885191; PubMed Central PMCID: PMC4035074.

49. Westenberger SJ, Cui L, Dharia N, Winzeler E, Cui L. Genome-wide nucleosome mapping of Plasmodium falciparum reveals histone-rich coding and histone-poor intergenic regions and chromatin remodeling of core and subtelomeric genes. BMC Genomics. 2009; 10:610. Epub 2009/12/18. https://doi.org/10.1186/1471-2164-10-610 PMID: 20015349; PubMed Central PMCID: PMC2801526.

50. Ponts N, Harris EY, Prudhomme J, Wick I, Eckhardt-Ludka C, Hicks GR, et al. Nucleosome landscape and control of transcription in the human malaria parasite. Genome Res. 2010; 20(2):228–38. Epub 2010/01/08. https://doi.org/10.1101/gr.101063.109 PMID: 20054063; PubMed Central PMCID: PMC2813478.

51. Kensche PR, Hoeijmakers WA, Toenhake CG, Bras M, Chappell L, Berriman M, et al. The nucleosome landscape of Plasmodium falciparum reveals chromatin architecture and dynamics of regulatory sequences. Nucleic Acids Res. 2016; 44(5):2110–24. Epub 2015/11/19. https://doi.org/10.1093/nar/gkv1214 PMID: 26578577; PubMed Central PMCID: PMC4797266.

52. Toenhake CG, Fraschka SA, Vijayabaskar MS, Westhead DR, van Heeringen SJ, Bartfai R. Chromatin Accessibility-Based Characterization of the Gene Regulatory Network Underlying Plasmodium falciparum Blood-Stage Development. Cell Host Microbe. 2018; 23(4):557–69 e9. Epub 2018/04/13. https://doi.org/10.1016/j.chom.2018.03.007 PMID: 29649445; PubMed Central PMCID: PMC5899830.

53. Gupta AP, Chin WH, Zhu L, Mok S, Luah YH, Lim EH, et al. Dynamic epigenetic regulation of gene expression during the life cycle of malaria parasite Plasmodium falciparum. PLoS Pathog. 2013; 9(2): e1003170. Epub 2013/03/08. https://doi.org/10.1371/journal.ppat.1003170 PMID: 23468622; PubMed Central PMCID: PMC3585154.

54. Bartfai R, Hoeijmakers WA, Salcedo-Amaya AM, Smits AH, Janssen-Megens E, Kaan A, et al. H2A.Z demarcates intergenic regions of the plasmodium falciparum epigenome that are dynamically marked by H3K9ac and H3K4me3. PLoS Pathog. 2010; 6(12):e1001223. Epub 2010/12/29. https://doi.org/10.1371/journal.ppat.1001223 PMID: 21187892; PubMed Central PMCID: PMC3002978.

55. Fan Q, An L, Cui L. Plasmodium falciparum histone acetyltransferase, a yeast GCN5 homologue involved in chromatin remodeling. Eukaryot Cell. 2004; 3(2):264–76. Epub 2004/04/13. https://doi.org/10.1128/EC.3.2.264-276.2004 PMID: 15075257; PubMed Central PMCID: PMC387650.

56. Cui L, Miao J, Furuya T, Li X, Su XZ, Cui L. PfGCN5-mediated histone H3 acetylation plays a key role in gene expression in Plasmodium falciparum. Eukaryot Cell. 2007; 6(7):1219–27. Epub 2007/04/24. https://doi.org/10.1128/EC.00062-07 PMID: 17449656; PubMed Central PMCID: PMC1951105.

57. Miao J, Fan Q, Cui L, Li X, Wang H, Ning G, et al. The MYST family histone acetyltransferase regulates gene expression and cell cycle in malaria parasite Plasmodium falciparum. Mol Microbiol. 2010; 78(4):883–902. Epub 2010/09/03. https://doi.org/10.1111/j.1365-2958.2010.07371.x PMID: 20807207; PubMed Central PMCID: PMC2978264.

58. Cui L, Fan Q, Miao J. Histone lysine methyltransferases and demethylases in Plasmodium falciparum. International journal for parasitology. 2008; 38(10):1083–97. Epub 2008/02/27. https://doi.org/10.1016/j.ijpara.2008.01.002 PMID: 18299133; PubMed Central PMCID: PMC4566933.

59. Xiao B, Yin S, Hu Y, Sun M, Wei J, Huang Z, et al. Epigenetic editing by CRISPR/dCas9 in Plasmodium falciparum. Proc Natl Acad Sci U S A. 2019; 116(1):255–60. Epub 2018/12/26. https://doi.org/10.1073/pnas.1813542116 PMID: 30584102; PubMed Central PMCID: PMC6320497.

60. Bhowmick K, Tehlan A, Sunita, Sudhakar R, Kaur I, Sijwali PS, et al. Plasmodium falciparum GCN5 acetyltransferase follows a novel proteolytic processing pathway that is essential for its function. J Cell Sci. 2020; 133(1). Epub 2019/12/22. https://doi.org/10.1242/jcs.236489 PMID: 31862795.

61. Cui L, Miao J, Furuya T, Fan Q, Li X, Rathod PK, et al. Histone acetyltransferase inhibitor anacardic acid causes changes in global gene expression during in vitro Plasmodium falciparum development. Eukaryot Cell. 2008; 7(7):1200–10. Epub 2008/05/20. https://doi.org/10.1128/EC.00063-08 PMID: 18487348; PubMed Central PMCID: PMC2446667.

62. Hoeijmakers WAM, Miao J, Schmidt S, Toenhake CG, Shrestha S, Venhuizen J, et al. Epigenetic reader complexes of the human malaria parasite, Plasmodium falciparum. Nucleic Acids Res. 2019; 47(22):11574–88. Epub 2019/11/16. https://doi.org/10.1093/nar/gkz1044 PMID: 31728527.

63. Fan Q, An L, Cui L. PfADA2, a Plasmodium falciparum homologue of the transcriptional coactivator ADA2 and its in vivo association with the histone acetyltransferase PfGCN5. Gene. 2004; 336(2):251–61. Epub 2004/07/13. https://doi.org/10.1016/j.gene.2004.04.005 PMID: 15246536.

64. Bischoff E, Vaquero C. In silico and biological survey of transcription-associated proteins implicated in the transcriptional machinery during the erythrocytic development of Plasmodium falciparum. BMC genomics. 2010; 11:34. Epub 2010/01/19. https://doi.org/10.1186/1471-2164-11-34 PMID: 20078850; PubMed Central PMCID: PMC2821373.

65. Schimanski B, Nguyen TN, Gunzl A. Highly efficient tandem affinity purification of trypanosome protein complexes based on a novel epitope combination. Eukaryot Cell. 2005; 4(11):1942–50. Epub 2005/11/10. https://doi.org/10.1128/EC.4.11.1942-1950.2005 PMID: 16278461; PubMed Central PMCID: PMC1287860.

66. Takebe S, Witola WH, Schimanski B, Gunzl A, Ben Mamoun C. Purification of components of the translation elongation factor complex of Plasmodium falciparum by tandem affinity purification. Eukaryotic cell. 2007; 6(4):584–91. Epub 2007/02/20. https://doi.org/10.1128/EC.00376-06 PMID: 17307963; PubMed Central PMCID: PMC1865644.

67. Miao J, Li X, Cui L. Cloning of Plasmodium falciparum by single-cell sorting. Experimental parasitology. 2010; 126(2):198–202. Epub 2010/05/04. https://doi.org/10.1016/j.exppara.2010.04.022 PMID: 20435038; PubMed Central PMCID: PMC2914851.

68. Teo G, Liu G, Zhang J, Nesvizhskii AI, Gingras AC, Choi H. SAINTexpress: improvements and additional features in Significance Analysis of INTeractome software. J Proteomics. 2014; 100:37–43. Epub 2014/02/12. https://doi.org/10.1016/j.jprot.2013.10.023 PMID: 24513533; PubMed Central PMCID: PMC4102138.

69. Singh M, D'Silva L, Holak TA. DNA-binding properties of the recombinant high-mobility-group-like AT-hook-containing region from human BRG1 protein. Biol Chem. 2006; 387(10–11):1469–78. Epub 2006/11/04. https://doi.org/10.1515/BC.2006.184 PMID: 17081121.

70. Darvekar S, Johnsen SS, Eriksen AB, Johansen T, Sjottem E. Identification of two independent nucleosome-binding domains in the transcriptional co-activator SPBP. Biochem J. 2012; 442(1):65–75. Epub 2011/11/16. https://doi.org/10.1042/BJ20111230 PMID: 22081970.

71. Sjottem E, Rekdal C, Svineng G, Johnsen SS, Klenow H, Uglehus RD, et al. The ePHD protein SPBP interacts with TopBP1 and together they co-operate to stimulate Ets1-mediated transcription. Nucleic Acids Res. 2007; 35(19):6648–62. Epub 2007/10/05. https://doi.org/10.1093/nar/gkm739 PMID: 17913746; PubMed Central PMCID: PMC2095823.

72. Avgousti DC, Cecere G, Grishok A. The conserved PHD1-PHD2 domain of ZFP-1/AF10 is a discrete functional module essential for viability in Caenorhabditis elegans. Mol Cell Biol. 2013; 33(5):999–1015. Epub 2012/12/25. https://doi.org/10.1128/MCB.01462-12 PMID: 23263989; PubMed Central PMCID: PMC3623080.

73. Liu Z, Li F, Ruan K, Zhang J, Mei Y, Wu J, et al. Structural and functional insights into the human Borjeson-Forssman-Lehmann syndrome-associated protein PHF6. J Biol Chem. 2014; 289(14):10069–83. Epub 2014/02/21. https://doi.org/10.1074/jbc.M113.535351 PMID: 24554700; PubMed Central PMCID: PMC3974978.

74. Sanchez R, Zhou MM. The PHD finger: a versatile epigenome reader. Trends Biochem Sci. 2011; 36 (7):364–72. Epub 2011/04/26. https://doi.org/10.1016/j.tibs.2011.03.005 PMID: 21514168; PubMed Central PMCID: PMC3130114.

75. Miao J, Lawrence M, Jeffers V, Zhao F, Parker D, Ge Y, et al. Extensive lysine acetylation occurs in evolutionarily conserved metabolic pathways and parasite-specific functions during Plasmodium falciparum intraerythrocytic development. Mol Microbiol. 2013; 89(4):660–75. Epub 2013/06/26. https://doi.org/10.1111/mmi.12303 PMID: 23796209; PubMed Central PMCID: PMC3757501.

76. LaCount DJ, Vignali M, Chettier R, Phansalkar A, Bell R, Hesselberth JR, et al. A protein interaction network of the malaria parasite Plasmodium falciparum. Nature. 2005; 438(7064):103–7. Epub 2005/11/04. https://doi.org/10.1038/nature04104 PMID: 16267556.

77. Josling GA, Petter M, Oehring SC, Gupta AP, Dietz O, Wilson DW, et al. A Plasmodium Falciparum Bromodomain Protein Regulates Invasion Gene Expression. Cell Host Microbe. 2015; 17(6):741–51. Epub 2015/06/13. https://doi.org/10.1016/j.chom.2015.05.009 PMID: 26067602.

78. Santos JM, Josling G, Ross P, Joshi P, Orchard L, Campbell T, et al. Red Blood Cell Invasion by the Malaria Parasite Is Coordinated by the PfAP2-I Transcription Factor. Cell Host Microbe. 2017; 21 (6):731–41 e10. Epub 2017/06/16. https://doi.org/10.1016/j.chom.2017.05.006 PMID: 28618269; PubMed Central PMCID: PMC5855115.

79. Zhang M, Wang C, Otto TD, Oberstaller J, Liao X, Adapa SR, et al. Uncovering the essential genes of the human malaria parasite Plasmodium falciparum by saturation mutagenesis. Science. 2018; 360

(6388). Epub 2018/05/05. https://doi.org/10.1126/science.aap7847 PMID: 29724925; PubMed Central PMCID: PMC6360947.

80. Miao J, Li J, Fan Q, Li X, Li X, Cui L. The Puf-family RNA-binding protein PfPuf2 regulates sexual development and sex differentiation in the malaria parasite Plasmodium falciparum. J Cell Sci. 2010; 123(Pt 7):1039–49. Epub 2010/03/04. https://doi.org/10.1242/jcs.059824 PMID: 20197405; PubMed Central PMCID: PMC2844316.

81. Bian C, Xu C, Ruan J, Lee KK, Burke TL, Tempel W, et al. Sgf29 binds histone H3K4me2/3 and is required for SAGA complex recruitment and histone H3 acetylation. EMBO J. 2011; 30(14):2829–42. Epub 2011/06/21. https://doi.org/10.1038/emboj.2011.193 PMID: 21685874; PubMed Central PMCID: PMC3160252.

82. Volz J, Carvalho TG, Ralph SA, Gilson P, Thompson J, Tonkin CJ, et al. Potential epigenetic regulatory proteins localise to distinct nuclear sub-compartments in Plasmodium falciparum. International journal for parasitology. 2010; 40(1):109–21. Epub 2009/09/22. https://doi.org/10.1016/j.ijpara.2009.09.002 PMID: 19765590.

83. Hassan AH, Prochasson P, Neely KE, Galasinski SC, Chandy M, Carrozza MJ, et al. Function and selectivity of bromodomains in anchoring chromatin-modifying complexes to promoter nucleosomes. Cell. 2002; 111(3):369–79. Epub 2002/11/07. https://doi.org/10.1016/s0092-8674(02)01005-x PMID: 12419247.

84. Vosnakis N, Koch M, Scheer E, Kessler P, Mely Y, Didier P, et al. Coactivators and general transcription factors have two distinct dynamic populations dependent on transcription. EMBO J. 2017; 36 (18):2710–25. Epub 2017/07/21. https://doi.org/10.15252/embj.201696035 PMID: 28724529; PubMed Central PMCID: PMC5599802.

85. Subramanian A, Tamayo P, Mootha VK, Mukherjee S, Ebert BL, Gillette MA, et al. Gene set enrichment analysis: a knowledge-based approach for interpreting genome-wide expression profiles. Proc Natl Acad Sci U S A. 2005; 102(43):15545–50. Epub 2005/10/04. https://doi.org/10.1073/pnas.0506580102 PMID: 16199517; PubMed Central PMCID: PMC1239896.

86. Mootha VK, Lindgren CM, Eriksson KF, Subramanian A, Sihag S, Lehar J, et al. PGC-1alpha-responsive genes involved in oxidative phosphorylation are coordinately downregulated in human diabetes. Nat Genet. 2003; 34(3):267–73. Epub 2003/06/17. https://doi.org/10.1038/ng1180 PMID: 12808457.

87. Ralph SA, Scheidig-Benatar C, Scherf A. Antigenic variation in Plasmodium falciparum is associated with movement of var loci between subnuclear locations. Proceedings of the National Academy of Sciences of the United States of America. 2005; 102(15):5414–9. Epub 2005/03/31. https://doi.org/10.1073/pnas.0408883102 PMID: 15797990; PubMed Central PMCID: PMC556247.

88. Dzikowski R, Li F, Amulic B, Eisberg A, Frank M, Patel S, et al. Mechanisms underlying mutually exclusive expression of virulence genes by malaria parasites. EMBO reports. 2007; 8(10):959–65. Epub 2007/09/01. https://doi.org/10.1038/sj.embor.7401063 PMID: 17762879; PubMed Central PMCID: PMC2002552.

89. Cowman AF, Berry D, Baum J. The cellular and molecular basis for malaria parasite invasion of the human red blood cell. J Cell Biol. 2012; 198(6):961–71. Epub 2012/09/19. https://doi.org/10.1083/jcb.201206112 PMID: 22986493; PubMed Central PMCID: PMC3444787.

90. Painter HJ, Campbell TL, Llinas M. The Apicomplexan AP2 family: integral factors regulating Plasmodium development. Molecular and biochemical parasitology. 2011; 176(1):1–7. Epub 2010/12/04. https://doi.org/10.1016/j.molbiopara.2010.11.014 PMID: 21126543; PubMed Central PMCID: PMC3026892.

91. Jeninga MD, Quinn JE, Petter M. ApiAP2 Transcription Factors in Apicomplexan Parasites. Pathogens. 2019; 8(2). Epub 2019/04/10. https://doi.org/10.3390/pathogens8020047 PMID: 30959972.

92. Flueck C, Bartfai R, Niederwieser I, Witmer K, Alako BT, Moes S, et al. A major role for the Plasmodium falciparum ApiAP2 protein PfSIP2 in chromosome end biology. PLoS pathogens. 2010; 6(2): e1000784. Epub 2010/03/03. https://doi.org/10.1371/journal.ppat.1000784 PMID: 20195509; PubMed Central PMCID: PMC2829057.

93. Josling GA, Russell TJ, Venezia J, Orchard L, van Biljon R, Painter HJ, et al. Dissecting the role of PfAP2-G in malaria gametocytogenesis. Nat Commun. 2020; 11(1):1503. Epub 2020/03/22. https://doi.org/10.1038/s41467-020-15026-0 PMID: 32198457; PubMed Central PMCID: PMC7083873.

94. Kafsack BF, Rovira-Graells N, Clark TG, Bancells C, Crowley VM, Campino SG, et al. A transcriptional switch underlies commitment to sexual development in malaria parasites. Nature. 2014; 507 (7491):248–52. Epub 2014/02/28. https://doi.org/10.1038/nature12920 PMID: 24572369; PubMed Central PMCID: PMC4040541.

95. Fraschka SA, Filarsky M, Hoo R, Niederwieser I, Yam XY, Brancucci NMB, et al. Comparative Heterochromatin Profiling Reveals Conserved and Unique Epigenome Signatures Linked to Adaptation and Development of Malaria Parasites. Cell Host Microbe. 2018; 23(3):407–20 e8. Epub 2018/03/06.

https://doi.org/10.1016/j.chom.2018.01.008 PMID: 29503181; PubMed Central PMCID: PMC5853956.

96. Jiang L, Mu J, Zhang Q, Ni T, Srinivasan P, Rayavara K, et al. PfSETvs methylation of histone H3K36 represses virulence genes in Plasmodium falciparum. Nature. 2013; 499(7457):223–7. Epub 2013/07/05. https://doi.org/10.1038/nature12361 PMID: 23823717; PubMed Central PMCID: PMC3770130.

97. Vermeulen M, Eberl HC, Matarese F, Marks H, Denissov S, Butter F, et al. Quantitative interaction proteomics and genome-wide profiling of epigenetic histone marks and their readers. Cell. 2010; 142 (6):967–80. Epub 2010/09/21. https://doi.org/10.1016/j.cell.2010.08.020 PMID: 20850016.

98. Li S, Shogren-Knaak MA. The Gcn5 bromodomain of the SAGA complex facilitates cooperative and cross-tail acetylation of nucleosomes. J Biol Chem. 2009; 284(14):9411–7. Epub 2009/02/17. https://doi.org/10.1074/jbc.M809617200 PMID: 19218239; PubMed Central PMCID: PMC2666593.

99. Govind CK, Zhang F, Qiu H, Hofmeyer K, Hinnebusch AG. Gcn5 promotes acetylation, eviction, and methylation of nucleosomes in transcribed coding regions. Mol Cell. 2007; 25(1):31–42. Epub 2007/01/16. https://doi.org/10.1016/j.molcel.2006.11.020 PMID: 17218269.

100. Nightingale KP, Gendreizig S, White DA, Bradbury C, Hollfelder F, Turner BM. Cross-talk between histone modifications in response to histone deacetylase inhibitors: MLL4 links histone H3 acetylation and histone H3K4 methylation. J Biol Chem. 2007; 282(7):4408–16. Epub 2006/12/15. https://doi.org/10.1074/jbc.M606773200 PMID: 17166833.

101. Milne TA, Briggs SD, Brock HW, Martin ME, Gibbs D, Allis CD, et al. MLL targets SET domain methyltransferase activity to Hox gene promoters. Mol Cell. 2002; 10(5):1107–17. Epub 2002/11/28. https://doi.org/10.1016/s1097-2765(02)00741-4 PMID: 12453418.

102. Chaal BK, Gupta AP, Wastuwidyaningtyas BD, Luah YH, Bozdech Z. Histone deacetylases play a major role in the transcriptional regulation of the Plasmodium falciparum life cycle. PLoS Pathog. 2010; 6(1):e1000737. Epub 2010/01/29. https://doi.org/10.1371/journal.ppat.1000737 PMID: 20107518; PubMed Central PMCID: PMC2809759.

103. Deitsch KW, Dzikowski R. Variant gene expression and antigenic variation by malaria parasites. Annual review of microbiology. 2017; 71:625–41. Epub 2017/07/13. https://doi.org/10.1146/annurev-micro-090816-093841 PMID: 28697665.

104. Lopez-Rubio JJ, Gontijo AM, Nunes MC, Issar N, Hernandez Rivas R, Scherf A. 5' flanking region of var genes nucleate histone modification patterns linked to phenotypic inheritance of virulence traits in malaria parasites. Mol Microbiol. 2007; 66(6):1296–305. Epub 2007/11/22. https://doi.org/10.1111/j.1365-2958.2007.06009.x PMID: 18028313; PubMed Central PMCID: PMC2228885.

105. Coleman BI, Skillman KM, Jiang RH, Childs LM, Altenhofen LM, Ganter M, et al. A Plasmodium falciparum histone deacetylase regulates antigenic variation and gametocyte conversion. Cell host & microbe. 2014; 16(2):177–86. Epub 2014/08/15. https://doi.org/10.1016/j.chom.2014.06.014 PMID: 25121747; PubMed Central PMCID: PMC4188636.

106. Duraisingh MT, Voss TS, Marty AJ, Duffy MF, Good RT, Thompson JK, et al. Heterochromatin silencing and locus repositioning linked to regulation of virulence genes in Plasmodium falciparum. Cell. 2005; 121(1):13–24. Epub 2005/04/12. https://doi.org/10.1016/j.cell.2005.01.036 PMID: 15820675.

107. Tonkin CJ, Carret CK, Duraisingh MT, Voss TS, Ralph SA, Hommel M, et al. Sir2 paralogues cooperate to regulate virulence genes and antigenic variation in Plasmodium falciparum. PLoS Biol. 2009; 7 (4):e84. Epub 2009/05/01. https://doi.org/10.1371/journal.pbio.1000084 PMID: 19402747; PubMed Central PMCID: PMC2672602.

108. Dastidar EG, Dzeyk K, Krijgsveld J, Malmquist NA, Doerig C, Scherf A, et al. Comprehensive histone phosphorylation analysis and identification of Pf14-3-3 protein as a histone H3 phosphorylation reader in malaria parasites. PloS one. 2013; 8(1):e53179. Epub 2013/01/12. https://doi.org/10.1371/journal.pone.0053179 PMID: 23308157; PubMed Central PMCID: PMC3538786.

109. Lo WS, Duggan L, Emre NC, Belotserkovskya R, Lane WS, Shiekhattar R, et al. Snf1—a histone kinase that works in concert with the histone acetyltransferase Gcn5 to regulate transcription. Science. 2001; 293(5532):1142–6. Epub 2001/08/11. https://doi.org/10.1126/science.1062322 PMID: 11498592

110. Kumar A, Bhowmick K, Vikramdeo KS, Mondal N, Subbarao N, Dhar SK. Designing novel inhibitors against histone acetyltransferase (HAT: GCN5) of Plasmodium falciparum. Eur J Med Chem. 2017; 138:26–37. Epub 2017/06/24. https://doi.org/10.1016/j.ejmech.2017.06.009 PMID: 28644986.

111. Moustakim M, Clark PG, Trulli L, Fuentes de Arriba AL, Ehebauer MT, Chaikuad A, et al. Discovery of a PCAF Bromodomain Chemical Probe. Angew Chem Int Ed Engl. 2017; 56(3):827–31. Epub 2016/12/15. https://doi.org/10.1002/anie.201610816 PMID: 27966810; PubMed Central PMCID: PMC5412877.

112. Trager W, Jensen JB. Human malaria parasites in continuous culture. Science. 1976; 193(4254):673–5. Epub 1976/08/20. https://doi.org/10.1126/science.781840 PMID: 781840.

113. Miao J, Cui L. Rapid isolation of single malaria parasite-infected red blood cells by cell sorting. Nat Protoc. 2011; 6(2):140–6. Epub 2011/02/05. https://doi.org/10.1038/nprot.2010.185 PMID: 21293455; PubMed Central PMCID: PMC3150729.

114. Fan Q, Miao J, Cui L. Characterization of PRMT1 from Plasmodium falciparum. The Biochemical journal. 2009; 421(1):107–18. Epub 2009/04/07. https://doi.org/10.1042/BJ20090185 PMID: 19344311.

115. Deitsch K, Driskill C, Wellems T. Transformation of malaria parasites by the spontaneous uptake and expression of DNA from human erythrocytes. Nucleic acids research. 2001; 29(3):850–3. Epub 2001/02/13. https://doi.org/10.1093/nar/29.3.850 PMID: 11160909; PubMed Central PMCID: PMC30384.

116. Miao J, Chen Z, Wang Z, Shrestha S, Li X, Li R, et al. Sex-Specific Biology of the Human Malaria Parasite Revealed from the Proteomes of Mature Male and Female Gametocytes. Mol Cell Proteomics. 2017; 16(4):537–51. Epub 2017/01/28. https://doi.org/10.1074/mcp.M116.061804 PMID: 28126901; PubMed Central PMCID: PMC5383777.

117. Perez-Riverol Y, Csordas A, Bai J, Bernal-Llinares M, Hewapathirana S, Kundu DJ, et al. The PRIDE database and related tools and resources in 2019: improving support for quantification data. Nucleic Acids Res. 2019; 47(D1):D442–D50. Epub 2018/11/06. https://doi.org/10.1093/nar/gky1106 PMID: 30395289; PubMed Central PMCID: PMC6323896.

118. Singh S, Alam MM, Pal-Bhowmick I, Brzostowski JA, Chitnis CE. Distinct external signals trigger sequential release of apical organelles during erythrocyte invasion by malaria parasites. PLoS Pathog. 2010; 6(2):e1000746. Epub 2010/02/09. https://doi.org/10.1371/journal.ppat.1000746 PMID: 20140184; PubMed Central PMCID: PMC2816683.

119. Shrestha S, Li X, Ning G, Miao J, Cui L. The RNA-binding protein Puf1 functions in the maintenance of gametocytes in Plasmodium falciparum. J Cell Sci. 2016; 129(16):3144–52. Epub 2016/07/08. https://doi.org/10.1242/jcs.186908 PMID: 27383769; PubMed Central PMCID: PMC5004898.

120. Miao J, Fan Q, Cui L, Li J, Li J, Cui L. The malaria parasite Plasmodium falciparum histones: organization, expression, and acetylation. Gene. 2006; 369:53–65. Epub 2006/01/18. https://doi.org/10.1016/j.gene.2005.10.022 PMID: 16410041.

121. Tonkin CJ, van Dooren GG, Spurck TP, Struck NS, Good RT, Handman E, et al. Localization of organellar proteins in Plasmodium falciparum using a novel set of transfection vectors and a new immunofluorescence fixation method. Molecular and biochemical parasitology. 2004; 137(1):13–21. Epub 2004/07/29. https://doi.org/10.1016/j.molbiopara.2004.05.009 PMID: 15279947.

122. Lucky AB, Sakaguchi M, Katakai Y, Kawai S, Yahata K, Templeton TJ, et al. Plasmodium knowlesi Skeleton-Binding Protein 1 Localizes to the 'Sinton and Mulligan' Stipplings in the Cytoplasm of Monkey and Human Erythrocytes. PLoS One. 2016; 11(10):e0164272. Epub 2016/10/13. https://doi.org/10.1371/journal.pone.0164272 PMID: 27732628; PubMed Central PMCID: PMC5061513.

123. Kim D, Langmead B, Salzberg SL. HISAT: a fast spliced aligner with low memory requirements. Nat Methods. 2015; 12(4):357–60. Epub 2015/03/10. nmeth.3317 [pii] https://doi.org/10.1038/nmeth.3317 PMID: 25751142.

124. Anders S, Huber W. Differential expression analysis for sequence count data. Genome biology. 2010; 11(10):R106. Epub 2010/10/29. https://doi.org/10.1186/gb-2010-11-10-r106 PMID: 20979621; PubMed Central PMCID: PMC3218662.

125. Liao Y, Smyth GK, Shi W. featureCounts: an efficient general purpose program for assigning sequence reads to genomic features. Bioinformatics. 2014; 30(7):923–30. Epub 2013/11/15. btt656 [pii] https://doi.org/10.1093/bioinformatics/btt656 PMID: 24227677.

126. Zhu L, Mok S, Imwong M, Jaidee A, Russell B, Nosten F, et al. New insights into the Plasmodium vivax transcriptome using RNA-Seq. Sci Rep. 2016; 6:20498–. https://doi.org/10.1038/srep20498 PMID: 26858037.

127. Livak KJ, Schmittgen TD. Analysis of relative gene expression data using real-time quantitative PCR and the 2(-Delta Delta C(T)) Method. Methods. 2001; 25(4):402–8. Epub 2002/02/16. https://doi.org/10.1006/meth.2001.1262 PMID: 11846609.